

DELFT UNIVERSITY OF TECHNOLOGY
FACULTY OF AEROSPACE ENGINEERING
AE3212-II
SIMULATION, VERIFICATION AND VALIDATION

Flight Dynamics Assignment

Development, Verification and Validation of a Flight Dynamics Simulation

Lecturer: Wouter van der Waal



March 29, 2022

Group B15

Oleksandr Krochak	5015529	Julie Paddeu	4997522
João Rodríguez	4993578	Oliver Ross	5008042
Lorenz Veithen	5075211	Niek Zandvliet	4796403

Contents

1	Introduction	1
2	Numerical Model	2
2.1	Reference Frames <i>Julie</i>	2
2.2	Equilibrium Equations <i>Lorenz, Julie</i>	2
2.3	Equations of Motion <i>Lorenz, Julie, Niek</i>	4
2.3.1	Assumptions Equations of Motion [1]	4
2.3.2	Non-Dimensional Linearised Equations of Motion	5
2.4	Eigenvalues of A_s and A_a <i>Julie</i>	6
2.5	Analytical Derivation of the Simplified Eigenvalues for the Different Eigenmotions <i>Julie, Oliver</i>	7
2.5.1	Symmetric Motions	7
2.5.2	Asymmetric Motions	9
2.6	Simulation <i>Lorenz</i>	10
3	Flight Data Processing	12
3.1	Flight Overview <i>Niek</i>	12
3.2	Mass and Balance <i>Julie, Niek</i>	12
3.2.1	Change of Total Aircraft Mass over Time	12
3.2.2	Change in the Center of Gravity over Time	13
3.3	Lift-Drag Polar <i>Lorenz, Joao</i>	14
3.4	Elevator Trim Curve Static Measurements <i>Joao</i>	15
3.4.1	Moment Coefficient due to Elevator C_{m_s}	16
3.4.2	Longitudinal Stability Coefficient C_{m_α}	16
3.4.3	Dimensionless Standard Thrust Coefficient T_{c_s}	17
3.4.4	Reduced Elevator Deflection ($\delta_{e_{eq}}^*$) and Reduced Stick Force (F_e^*)	17
3.5	Dynamic Measurements Processing <i>Alex</i>	18
3.5.1	Flight Data Analysis	18
3.5.2	Flight Data Non-Dimensionalisation	19
4	Verification	20
4.1	Verification of Unit Converters and Reduction of Measured Airspeed <i>Oliver</i>	20
4.2	Verification of Mass and Center of Gravity Calculation <i>Julie, Niek</i>	21
4.3	Verification of Data Processing Calculations <i>Joao</i>	21
4.3.1	Processing of First Stationary Series of Measurements	21
4.3.2	Processing of Second Stationary Series of Measurements	22
4.4	Verification of Recorded Data <i>Lorenz</i>	22
4.5	Verification of State Space Model and Simplified Eigenmotions <i>Julie, Oliver, Niek</i>	23
4.6	Global Tests	25
4.6.1	SYS-GLOBAL-001: Initial Value Problem <i>Alex, Julie</i>	25
4.6.2	SYS-GLOBAL-002: Sensitivity to Input Values <i>Lorenz</i>	26
4.7	Test Accuracy <i>Julie, Oliver, Joao, Lorenz, Niek</i>	27
5	Validation	28
5.1	Comparison of Graphs for Experimental and Simulation Data <i>Julie, Alex</i>	28
5.2	Comparison of Eigenmotion Parameters of Experimental Data and Numerical Model Output <i>Alex, Julie</i>	30
5.3	Improvement of Numerical Model: Model Matching <i>Oliver, Joao</i>	31
5.4	Reflection Numerical Model <i>Alex</i>	32
6	Conclusion <i>Alex</i>	34
References		

Introduction 1

Recently, the global economy has seen exponential growth. An increasing amount of companies operates outside their countries borders, resulting in more international meetings. These meetings were mostly held online due to the recent Covid-19 pandemic. Now that this pandemic is over, there is again an increasing demand for small business jets that can bring people quickly to the desired location without any delays and waiting time that comes with regular air travel. To ensure that all essential staff can come along, the aircraft has to seat ten people, including two pilots.

This report aims to create, verify and validate a simplified flight dynamic model that can represent and predict the dynamic behavior of an aircraft due to inputs on the ailerons, elevator and rudder. Data that is gathered during a test flight of the prototype aircraft will be used to increase the accuracy of the parameters of the model.

The report presented has the following structure. First the derivation and assumptions of the numerical model will be discussed in Chapter 2. The processing of the acquired flight data and the derivation of stability parameters will be discussed in Chapter 3. This verification of the numerical model, consisting of unit, subsystem and system tests, is presented in Chapter 4. Finally, the validation, consisting of both a graphical and numerical comparison between the experimental data and numerical data, is discussed in Chapter 5.

Table 1.1: Task Distribution

Task Description	Member	Hours/member
Coding		
Input dictionaries	Lorenz, Alex, João, Oliver	4
Flight data post-processing (ref. and own data)	Alex	20
Unit Conversion	Oliver	4
Parameter Reductions	Oliver, João	4
Mass & CG	Julie, Niek	8
$C_L - C_D$	Lorenz	3
Thrust Calculations	João, Lorenz	4
$C_{D_0}, e, C_{L_\alpha}, \alpha_{L=0}$	Lorenz	1
$F_e^* - \tilde{V}_e$ and $\delta_e \cdot \tilde{V}_e$	João	8
$C_{m_\alpha} & C_{m_\delta}$	Lorenz, João	4
State Space System	Lorenz	4
Simulation	Lorenz	8
Model Matching	Oliver, João	4
Verification Codes		
Verification mass & CG	Julie	4
Verification State Space System	Julie	2
Verification Unit Conversion and Reduction	Oliver	4
Eigenvalues and Eigenmotions	Julie, Oliver, Niek	8
Initial Value Response	Julie	2
Sensitivity	Lorenz	4
Recorded data	Lorenz	2
Data Processing	João	3
Reporting		
See report sections		36
V&V plan	Oliver, João, Niek	12

Numerical Model 2

Before describing the Equilibrium Equations and the Equations of Motion (EoM), the reference frames used will be discussed, in Section 2.1. Subsequently, the Equilibrium Equations and the EoM are presented in Section 2.2, and Section 2.3 respectively. However, the full derivation of the Equilibrium Equations, and EoM are presented in [1]. Then, the derivation of the eigenvalues for both the symmetric and asymmetric EoM will be described in Section 2.4. Finally, also the analytical derivation of the simplified eigenvalues for the different eigenmotions, with the used assumptions, is presented in Section 2.5.

2.1 Reference Frames *Julie*

The three reference frames used in this report are the stability reference frame, the body-fixed reference frame, and the vehicle reference frame. The latter is used for the Equilibrium Equations, while the body-fixed reference frame and the stability reference frame are used for the experimental data, and the EoM respectively. The body-fixed and stability reference frame have parallel Y-axis and coinciding origins at the centre of mass of the vehicle. However, the difference between these two reference frames is in how the X- and Z-axes are defined. More specifically, X_b lays in the symmetry plane of the aircraft and points in the direction of the nose of the aircraft, while X_s also lays in the symmetry plane of the aircraft but is pointing in the direction of the incoming airflow. Moreover, this difference between the X-axis results subsequently in a difference between the Z-axis, equal to the angle of attack, α [1]. This can be seen in Figure 2.1.

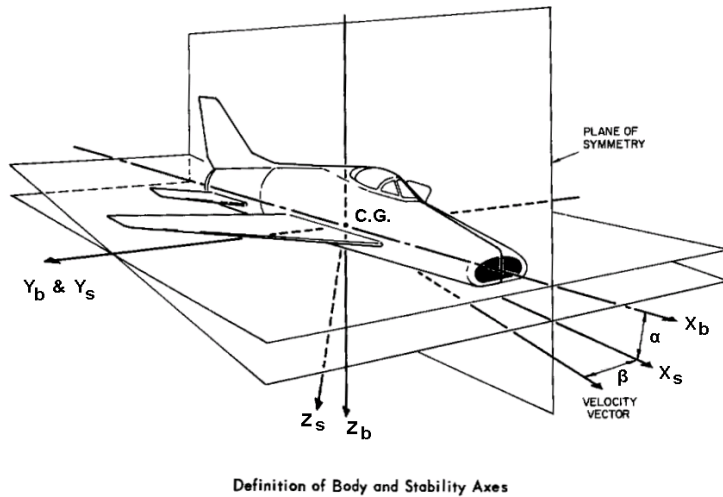


Figure 2.1: Difference between the body-fixed and stability reference frame [2].

Now, that the difference between the body-fixed reference frame and the stability reference frame is clear. It should be noticed that when using the stability reference frame to describe the EoM, $u_0 = V$ and $w_0 = 0$. Furthermore, the angle of attack measured relative to X_s in steady condition is equal to zero, $\alpha_0 = 0$, which leads to $\theta_0 = \gamma_0$.

Finally, the vehicle reference frame has the exact same orientation as the body-fixed reference frame, but has its origin at an arbitrary point, and not in the centre of gravity of the vehicle.

2.2 Equilibrium Equations *Lorenz, Julie*

For the first two stationary measurements, the equilibrium equations of horizontal, stationary and symmetric flight are derived to further analyse the stability of the aircraft. In this case it is valid to assume a horizontal, steady, symmetric

flight, since during the measurements, it was seen that the deviations in speed and altitude were negligible. However, this leads to the fact that $\frac{dV}{dt}$ and $\frac{d\gamma}{dt}$ are zero. Furthermore, γ is also assumed to be small. Knowing this, small angle approximations can be used, which leads to the linearization of the terms in the equilibrium equations, which include γ . Figure 2.2 presents the Free Body Diagram (FBD) in steady, straight and symmetric flight in; from this the equilibrium equations for the stationary measurements can be derived.

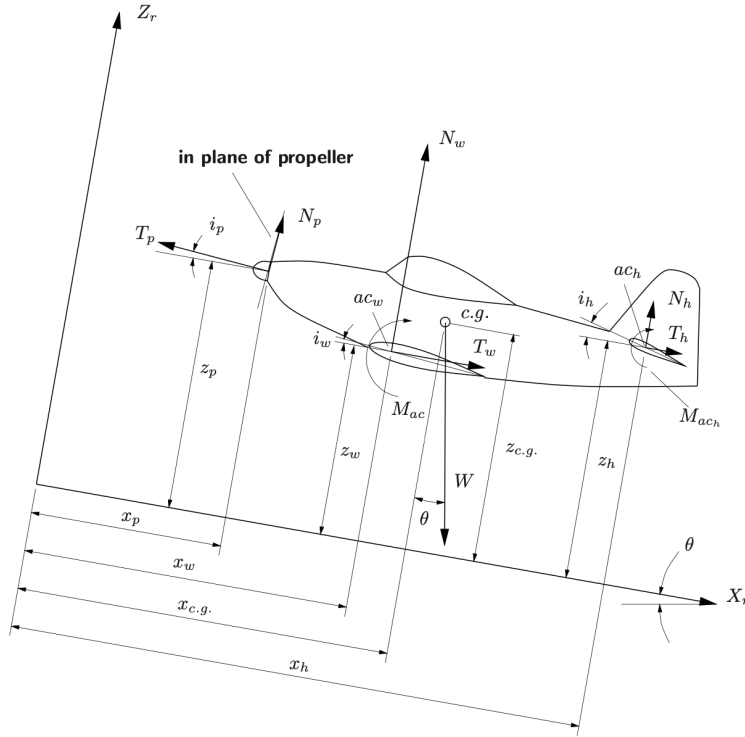


Figure 2.2: FBD in steady, straight and symmetric flight configuration [1]

Based on Figure 2.2, the equilibrium equations for the two sets of stationary measurements are obtained based on the following general assumptions [1]:

- **GSA-01 Symmetric horizontal stabilizer.** The airfoil of the horizontal stabilizer can be considered symmetric, such that M_{ac_h} can be neglected.
- **GSA-02 T_h contribution.** The contribution of T_h to the force in the X_B -direction and to the moment equation can be neglected. This assumption is nearly always valid due to the relatively small magnitude of this component with respect to the other forces.
- **GSA-03 T_w contribution.** The contribution of the T_w component is neglected in the moment equation. Such assumption is valid for small angles of attack, as is the case for the horizontal flight configuration discussed.
- **GSA-04 Engines alignment.** The engines are assumed to be aligned with the aircraft body axis, therefore i_p is zero. Furthermore, note that the engines of the Cessna Citation II (C550) used are at the back of the aircraft.
- **GSA-05 C_{N_p} contribution.** The contribution of the vertical component of the engine is considered very small compared to the thrust itself and is neglected in all equations.

This yields the set of non-dimensionalised equations shown in Equation 2.1.

$$\begin{aligned}
 C_T &= C_{T_w} - T_c \frac{2D^2}{S} = 0 \\
 C_N &= C_{N_w} + C_{N_h} \left(\frac{V_h}{V} \right)^2 \frac{S_h}{S} = \frac{W}{\frac{1}{2} \rho V^2 S} \\
 C_m &= C_{m_{ac}} + C_{N_w} \frac{x_{c.g.} - x_w}{\bar{c}} - C_{T_w} \frac{z_{c.g.} - z_w}{\bar{c}} + C_{N_h} \left(\frac{V_h}{V} \right)^2 \frac{S_h}{S} \frac{x_{c.g.} - x_h}{\bar{c}} + T_c \frac{2D^2}{S} \frac{z_{c.g.} - z_p}{\bar{c}} = 0
 \end{aligned} \tag{2.1}$$

However, some specific assumptions related to both the sets of stationary measurements are made, with **S1A**, and **S2A** referring to assumptions for the first and second set of stationary measurements respectively.

- **S1A-01** It is assumed that the sideslip angle is zero. This is valid, since zero wind velocity was previously assumed. The result of this is that the velocity vector is aligned with the flight direction, thus with the plane of symmetry.
- **S2A-01** It is assumed that the thrust is constant per measurement. This is valid, since the altitude is assumed to be constant for each measurement. Small deviations in thrust are neglected by making this assumption.
- **S2A-02** It is assumed that the configuration of the aircraft is not changing during the measurement. This is valid since the deviations in the elevator and trim deflection, and the angle of attack were negligible. This results in constant lift and drag coefficients for both wing and tail.
- **S2A-03** It is assumed that the force needed to overcome the friction in the control mechanism, F_{e_f} . This is a valid assumption, since a lot of effort is put into the minimization of this friction by the aircraft manufacturer. However, this leads to the fact that measurements are only accurate within the range $\pm F_{e_f}$.

2.3 Equations of Motion *Lorenz, Julie, Niek*

When looking at the dynamic response of the aircraft, the EoM have to be defined. However, before taking a closer look at the EoM, the assumptions used for the derivation will be presented, along with a discussion on their validity and effect.

2.3.1 Assumptions Equations of Motion [1]

- **GA-01** It is assumed that the vehicle is a rigid body of constant mass. This assumption is only true if there is no fuel flow and if there are no vehicle elastic modes. If indeed the mass of the aircraft is constant, this will lead to a constant matrix of inertia.
- **GA-02** A flat Earth is assumed. This assumption is valid in case the duration of the motions is short, since in that case the effect of the curvature of the Earth negligible. Making this assumption, the vehicle carried normal Earth reference frame will coincide with the normal Earth fixed reference frame.
- **GA-03** It is assumed that the Earth is non-rotating. In case the Coriolis and centripetal acceleration components are removed from the simulation inputs, this assumption can be used. Furthermore, the time-span of the motion should be kept short in order to avoid large errors. By assuming a non-rotating Earth the angular velocity of the Earth is neglected, and the Coriolis and centripetal accelerations are omitted. This can lead to large errors if the time-span of the motions is in the order of hours.
- **GA-04** It is assumed that the vehicle has a plane of symmetry. This is a valid assumption since the aircraft can be assumed to be symmetrical, apart from small components such as pitot tubes. However, these differences are small compared to the size of the entire aircraft and can therefore be neglected. By making this assumption, I_{xy} and I_{yz} will be zero when the body-fixed reference frame is aligned with the principal axis of the aircraft.
- **GA-05** It is assumed that the wind velocity is zero. Using the zero wind velocity allows for comparisons to be made between different aircraft and manoeuvres. Wind conditions change every second, thus trying to simulate with these wind conditions gives a different outcome every time. The kinematic velocity is equal to the aerodynamic velocity by using this assumption.
- **GA-06** It is assumed that the resultant thrust lies in the symmetry plane. This assumption is only true if the engines are aligned with the plane of symmetry. This assumption leads to the fact that the thrust only affects the symmetric aerodynamic forces and moments.
- **GA-07** It is assumed that the thrust is parallel to the velocity vector. This is a valid assumption since α_T is generally small. This assumption leads to a misalignment of the thrust vector compared to reality, since α_T is set to zero, and can therefore lead to some discrepancies. However, this assumption leads to further simplifications of the EoM, which is beneficial.
- **GA-08** It is assumed that the gravity field is constant. The percentage change between the gravity at sea level and the gravity at FL450 (ceiling of our ACFT¹), is negligible. Furthermore, measurements showed that the change in the gravity field over the Netherlands is negligible [3]. By using this assumption, there can be a discrepancy in the weight.

¹ACFT - aircraft

- **GA-09** It is assumed that the mass stays constant during the measurements. This is a valid assumption since the performed eigenmotions were of short duration, such that the difference in mass due to the fuel assumption is small and can therefore be neglected. However, this will lead to small deviations in some stability derivatives, since some of them are directly related to the mass of the aircraft.
- **GA-10** It is assumed that the wing area, S , stays constant during the whole flight. This is a valid assumption since the deflection of the control surfaces were small during the flight. The impact of the deflection on the total surface area is therefore small and clearly negligible.
- **GA-11** A linear model will be used. This assumption was discussed in [1], where it was shown that the aircraft response around an equilibrium state is reasonably well described by the linearized EoM. This assumption has a direct effect on the range of application of the simulation, limiting it to small disturbances and small angles.

2.3.2 Non-Dimensional Linearised Equations of Motion

Now that the assumptions are presented, the non-dimensionalised linearized Equations of Motion chosen to describe the aircraft dynamics in this work are presented. These were derived in [1, p.57-113] under the assumptions presented above. Furthermore, Equations 2.2 and 2.3 describe the EoM for the symmetric and asymmetric case, respectively.

$$\begin{bmatrix} C_{x_u} - 2\mu_c D_c & C_{x_\alpha} & C_{z_0} & C_{X_q} \\ C_{z_u} & C_{Z_\alpha} + (C_{Z_\alpha} - 2\mu_c) D_c & -C_{X_0} & C_{Z_q} - 2\mu_c \\ 0 & 0 & -D_c & 1 \\ C_{m_u} & C_{m_\alpha} + C_{m_\alpha} D_c & 0 & C_{m_q} - 2\mu_q K_{yy}^2 D_c \end{bmatrix} \begin{bmatrix} \hat{u} \\ \alpha \\ \theta \\ \frac{q\bar{c}}{V} \end{bmatrix} = \begin{bmatrix} -C_{X_\delta} \\ -C_{Z_\delta} \\ 0 \\ -C_{m_\delta} \end{bmatrix} \delta_e \quad (2.2)$$

$$\begin{bmatrix} C_{Y_\beta} + (C_{Y_\beta} - 2\mu_b) D_b & C_L & C_{Y_p} & C_{Y_r} - 4\mu_b \\ 0 & \frac{-1}{2} D_b & 1 & 0 \\ C_{l_\beta} & 0 & C_{l_p} - 4\mu_b K_{xx}^2 D_b & C_{l_r} + 4\mu_b K_{xz} D_b \\ C_{n_\beta} + C_{n_\beta} D_b & 0 & C_{n_p} + 4\mu_b K_{xz} D_b & C_{n_r} - 4\mu_b K_{zz}^2 D_b \end{bmatrix} \begin{bmatrix} \beta \\ \phi \\ \frac{pb}{2V} \\ \frac{rb}{2V} \end{bmatrix} = \begin{bmatrix} -C_{y_{\delta_a}} \\ 0 \\ -C_{l_{\delta_a}} \\ -C_{n_{\delta_a}} \end{bmatrix} \delta_a + \begin{bmatrix} -C_{y_{\delta_r}} \\ 0 \\ -C_{l_{\delta_r}} \\ -C_{n_{\delta_r}} \end{bmatrix} \delta_r \quad (2.3)$$

All the symbols used in those sets of equations are defined in [1, 4]. It is noted that $D_c = \frac{\bar{c}}{V} \frac{d}{dt}$ and $D_b = \frac{b}{V} \frac{d}{dt}$ are differential operators.

Now to be able to solve the EoM these systems can be rewritten in a space state form given by $\dot{\vec{x}} = A\vec{x} + B\vec{u}$ and $\vec{y} = C\vec{x} + D\vec{u}$, as shown in [4, p.20-21]. For both the symmetric and asymmetric case, the matrices C and D are the identity and the zero matrix of size, 4×4 respectively. Moreover, matrices A_s , A_a , B_s and B_a are obtained by rewriting Equations 2.2 and 2.3 in the form given by Equation 2.4 [1].

$$C_1 \dot{\vec{x}} + C_2 \vec{x} + C_3 \vec{u} = 0 \quad (2.4)$$

For the symmetric case, C_{1_s} , C_{2_s} and C_{3_s} are given by [1]:

$$C_{1_s} = \frac{\bar{c}}{V} \begin{bmatrix} -2\mu_c & 0 & 0 & 0 \\ 0 & (C_{Z_\alpha} - 2\mu_c) & 0 & 0 \\ 0 & 0 & -1 & 0 \\ 0 & C_{m_\alpha} & 0 & -2\mu_c K_{yy}^2 \end{bmatrix} \quad C_{2_s} = \begin{bmatrix} C_{x_u} & C_{x_\alpha} & C_{z_0} & C_{X_q} \\ C_{z_u} & C_{Z_\alpha} & -C_{X_0} & C_{Z_q} - 2\mu_c \\ 0 & 0 & 0 & 1 \\ C_{m_u} & C_{m_\alpha} & 0 & C_{m_q} \end{bmatrix} \quad C_{3_s} = \begin{bmatrix} C_{X_\delta} \\ C_{Z_\delta} \\ 0 \\ C_{m_\delta} \end{bmatrix}$$

With $x = [\hat{u} \quad \alpha \quad \theta \quad \frac{q\bar{c}}{V}]^T$ and $\vec{u} = [\delta_e]$.

Subsequently, for the asymmetric case, C_{1_a} , C_{2_a} and C_{3_a} are given by [1]:

$$C_{1_a} = \frac{\bar{b}}{V} \begin{bmatrix} (C_{Y_\beta} - 2\mu_b) & 0 & 0 & 0 \\ 0 & \frac{-1}{2} & 0 & 0 \\ 0 & 0 & -4\mu_b K_{xx}^2 & 4\mu_b K_{xz} \\ C_{n_\beta} & 0 & 4\mu_b K_{xz} & -4\mu_b K_{zz}^2 \end{bmatrix} \quad C_{2_a} = \begin{bmatrix} C_{Y_\beta} & C_L & C_{Y_p} & C_{Y_r} - 4\mu_b \\ 0 & 0 & 1 & 0 \\ C_{l_\beta} & 0 & C_{l_p} & C_{l_r} \\ C_{n_\beta} & 0 & C_{n_p} & C_{n_r} \end{bmatrix} \quad C_{3_a} = \begin{bmatrix} C_{y_{\delta_a}} & C_{y_{\delta_r}} \\ 0 & 0 \\ C_{l_{\delta_a}} & C_{l_{\delta_r}} \\ C_{n_{\delta_a}} & C_{n_{\delta_r}} \end{bmatrix}$$

With $x = [\beta \quad \phi \quad \frac{pb}{2V} \quad \frac{rb}{2V}]^T$ and $\vec{u} = [\delta_a \quad \delta_e]^T$. Following the guidelines presented in [4], the matrices A and B can be obtained from $A = -C_1^{-1}C_2$ and $B = -C_1^{-1}C_3$. This can be straightforwardly implemented directly in either Python or Matlab [1].

2.4 Eigenvalues of A_s and A_a

Now the dynamic response of the aircraft can be captured by the eigenvalues of the system. Therefore, in this section the non-dimensional eigenvalues of A_s and A_a will be analytically derived. Firstly, a closer look will be taken at the analytical derivation of the non-dimensional eigenvalues for the symmetric equations of motion given by Equation 2.2, after which they will be derived for the asymmetric equations of motion given by Equation 2.3.

The solution of the homogeneous equations for the symmetric motions is of the form presented in Equation 2.5 [1].

$$x = A_x e^{\lambda_c s_c} \quad (2.5)$$

In Equation 2.5, x is the representative for any of the components of motion, and s_c is the non-dimensional time, presented in Equation 2.6. Furthermore, the coefficient A_x in Equation 2.5 is partially determined by the initial conditions used in the equations of motion. Finally, it has to be noted that the variable λ_c is either real or complex and determines entirely, and only, the stability of the system. Therefore, it is important to find the eigenvalues in order to study the stability [1].

$$s_c = \frac{V}{\bar{c}} t \quad (2.6)$$

Before, substitution Equation 2.5 into Equation 2.2 in order to find the values of λ_c it has to be realized that in Equation 2.2 [1],

$$D_c x = \frac{\bar{c}}{V} \frac{d}{dt} (A_x e^{\lambda_c \frac{V}{\bar{c}} t}) = \lambda_c x \quad (2.7)$$

Now the result of the substitution is presented by Equation 2.8 [1]

$$\begin{bmatrix} C_{x_u} - 2\mu_c \lambda_c & C_{x_\alpha} & C_{z_0} & C_{X_q} \\ C_{z_u} & C_{Z_\alpha} + (C_{Z_\alpha} - 2\mu_c) \lambda_c & -C_{X_0} & C_{Z_q} - 2\mu_c \\ 0 & 0 & -\lambda_c & 1 \\ C_{m_u} & C_{m_\alpha} + C_{m_\alpha} \lambda_c & 0 & C_{m_q} - 2\mu_q K_{yy}^2 \lambda_c \end{bmatrix} \begin{bmatrix} A_u \\ A_\alpha \\ A_\theta \\ A_q \end{bmatrix} e^{\lambda_c s_c} = 0 \quad (2.8)$$

A more compact notation of Equation 2.8 is shown by Equation 2.9, in which $[\Delta]$ represents the characteristic matrix and \underline{A} , the vector containing the element A_u , A_α , A_θ , and A_q [1].

$$[\Delta] \underline{A} e^{\lambda_c s_c} = 0 \quad (2.9)$$

In this equation, however, the non-zero factor $e^{\lambda_c s_c}$ can be omitted without influencing the values for λ_c , which leads to Equation 2.10 [1].

$$[\Delta] \underline{A} = 0 \quad (2.10)$$

Furthermore, since the trivial solution will not be considered, since it corresponds with the original equilibrium flight condition, which is a separate particular case of disturbed motion, the matrix can only be solved in case the equations are dependent, in other words when the determinant of the square matrix $[\Delta]$, the characteristic determinant, is equal to zero. From this the non-dimensional eigenvalues, λ_c of the differential equations can be found. Finally, the results of the characteristic equation can be written as [1],

$$A\lambda_c^4 + BA\lambda_c^3 + CA\lambda_c^2 + DA\lambda_c + E = 0 \quad (2.11)$$

The coefficients of this characteristic equation can be found in [1]. However, it should be noticed that these coefficients are determined by assuming $C_{X_q} = 0$, since this stability derivative is very small [1].

Now, that the eigenvalues of the symmetric equations of motion, λ_c , are derived, the analytical derivation of the eigenvalues for the asymmetric equations of motion, λ_b , will be presented. The asymmetric equations of motion are shown by Equation 2.3. However, by discarding the terms due to the control surface deflections, the equation becomes homogeneous. Furthermore, it was found that $D_c x = \lambda_c x$. By filling this in the homogeneous form of the asymmetric equation of motion and setting the characteristic determinant equal to zero Equation 2.12 is obtained [1].

$$\begin{vmatrix} C_{Y_\beta} + (C_{Y_\beta} - 2\mu_b) \lambda_b & C_L & C_{Y_p} & C_{Y_r} - 4\mu_b \\ 0 & \frac{-1}{2} \lambda_b & 1 & 0 \\ C_{l_\beta} & 0 & C_{l_p} - 4\mu_b K_{xx}^2 \lambda_b & C_{l_r} + 4\mu_b K_{xz} \lambda_b \\ C_{n_\beta} + C_{n_\beta} \lambda_b & 0 & C_{n_p} + 4\mu_b K_{xz} \lambda_b & C_{n_r} - 4\mu_b K_{zz}^2 \lambda_b \end{vmatrix} = 0 \quad (2.12)$$

Using the assumption that C_{Y_β} and C_{n_β} are usually neglected the determinant can be rewritten as a quartic characteristic equation, presented by Equation 2.13, from which the non-dimensional eigenvalues can be computed [1].

$$A\lambda_b^4 + BA\lambda_b^3 + CA\lambda_b^2 + DA\lambda_b + E = 0 \quad (2.13)$$

Again, the coefficient of this characteristic equation can be found in [1].

2.5 Analytical Derivation of the Simplified Eigenvalues for the Different Eigenmotions

Julie, Oliver

The determination of the complete Equations of Motion and resulting characteristic equations will allow for the aircraft eigenmotions to be determined numerically with the use of Python software and the NumPy library. To ensure that these numerical results are consistent with the underlying model, a set of analytical motions should also be determined.

This section is split into two key subsections. First, Subsection 2.5.1 will analytically determine the eigenvalues for the symmetric eigenmotions. Subsequently, Subsection 2.5.2 will describe the analytical derivation of the eigenvalues for the asymmetric eigenmotions. In both subsections, the simplifying assumptions which were used will also be stated, with a brief justification for the assumptions, and their effects.

2.5.1 Symmetric Motions

In order to determine the eigenmotions which drive the motion of the aircraft throughout symmetric motions, the solutions of the complete equations of motion (as described in Equation 2.8), and the resulting characteristic equation (as described in Equation 2.11) must be determined. However, given that there is no analytical means to solve a fourth order polynomial (apart from trial and error, which is tedious and potentially inaccurate), some simplifying assumptions need to be made to reduce the degree of the equation (generally to degree two). These assumptions differ between various aircraft motions, therefore, each motion must be treated as a separate case. As such, Subsubsection 2.5.1 treats the short period motion, while Subsubsection 2.5.1 treats the phugoid motion.

Short Period Motion

The short period motion in an aircraft is determined by exerting a sudden pitching motion on the aircraft. In the case of the flight test, this was done by imposing a sudden pitch up motion on the aircraft using the elevators. The resulting motion of this is an oscillatory motion along the longitudinal axis of the aircraft, with the motion quickly damping out. As a result of this motion, three key assumptions can be made, each of which is built upon the previous ones. The first assumption which was made consists of two parts: prior to the change in pitch angle, the aircraft is in steady, level flight, and, following the change in pitch angle, there is no change in the velocity of the aircraft. The assumption of initially steady flight prior to the manoeuvre is consistent with the flight profile of the aircraft which was taking place during the flight test, thereby making the assumption justifiable. Additionally, the assumption of constant velocity is also justifiable given the extremely short time duration of the response of the aircraft following the change in pitch angle (hence the name, short period) [1].

By making use of this first assumption, there are a number of important effects which take place in Equation 2.8. Firstly, given the assumption of steady level flight, this implies that the flight path angle, γ , is zero and therefore, the pitch angle of the aircraft should also be zero. This leads to the stability derivative C_{X_0} being equal to zero as well, and therefore, the kinematic equation for the pitch angle may be dropped. Secondly, given that the velocity remains constant, there is no acceleration and therefore, there may not be any force along the X-direction which accelerates the aircraft. As a result of this, there is no need to solve the first row of the matrix corresponding to the force along the x-direction, and the column corresponding to the coefficients of \dot{u} may also be neglected as \dot{u} is also zero [1].

With the effects of the assumptions put in place, the updated matrix containing the equations of motion is shown below [1]:

$$\begin{bmatrix} C_{Z_\alpha} + (C_{Z\dot{\alpha}} - 2\mu_c)\lambda_c & C_{Z_q} + 2\mu_c \\ C_{m_\alpha} + C_{m\dot{\alpha}}\lambda_c & C_{m_q} - 2\mu_c K_Y^2 \lambda_c \end{bmatrix} \begin{bmatrix} \alpha \\ \frac{q\bar{c}}{V} \end{bmatrix} = 0 \quad (2.14)$$

and therefore, the resulting characteristic equation to be solved is [1]:

$$A\lambda_c^2 + B\lambda_c + C = 0 \quad (2.15)$$

where:

$$A = 2\mu_c K_Y^2 (2\mu_c - C_{Z_\alpha}) \quad (2.16)$$

$$B = -2\mu_c K_Y^2 C_{Z_\alpha} - (2\mu_c + C_{Z_q}) C_{m_\alpha} - (2\mu_c - C_{Z\dot{\alpha}}) C_{m_q} \quad (2.17)$$

$$C = C_{Z_\alpha} C_{m_q} - (2\mu_c + C_{Z_q}) \quad (2.18)$$

Solving for the eigenvalues can be easily done analytically by making use of the quadratic formula [1].

Despite the vast simplifications already imposed by the first assumption, there are further simplifications which may be added which do not significantly compromise the overall results. The second assumption which may be taken is the

following: the stability derivatives C_{Z_q} and $C_{Z_{\dot{\alpha}}}$ are negligible in comparison to the mass parameter $2\mu_c$, therefore the terms $(2\mu_c - C_{Z_{\dot{\alpha}}}) + (2\mu_c + C_{Z_q})$ can be reduced. This leads to a new set of coefficients for the characteristic polynomial, as shown below [1]:

$$A = 4\mu_c^2 K_Y^2 \quad (2.19)$$

$$B = -2\mu_c(K_Y^2 C_{Z_{\alpha}} + C_{m_{\dot{\alpha}}} + C_{m_q}) \quad (2.20)$$

$$C = C_{Z_{\alpha}} C_{m_q} - 2\mu_c C_{m_{\alpha}} \quad (2.21)$$

The last assumption which can be made regarding the short period is also the strongest one: that the aircraft's trajectory moves in a straight line. As a result of this, the centre of gravity of the aircraft will only move in a horizontal line, and therefore the Z-forces would be balanced. This introduces a brand-new set of implications, as now on top of the previously determined the equilibrium equation for the Z-force may now be dropped. As such, the originally four by four EOM matrix has now been completely reduced to the following [1]:

$$\begin{bmatrix} C_{m_{\alpha}} + C_{m_{\dot{\alpha}}} D_c & C_{m_q} - 2\mu_c K_Y^2 D_c \end{bmatrix} \begin{bmatrix} \alpha \\ \frac{q\bar{c}}{V} \end{bmatrix} = 0 \quad (2.22)$$

In addition to this, given the centre of gravity only moves horizontally, the flight path angle must therefore be zero. As a result of this, the pitch angle of the aircraft must be the same as its angle of attack. This is a significant result, as it is known that [1]:

$$D_c \frac{q\bar{c}}{V} = D_c^2 \theta \quad (2.23)$$

Therefore, the column vector as shown in the previous equation reduces to the following [1]:

$$\begin{bmatrix} \theta \\ \theta \end{bmatrix} \quad (2.24)$$

Because each term in the EOM matrix is multiplied by θ and the right-hand side of the equation remains zero, this factor can now be removed completely from the final characteristic equation. The result of this is shown below [1]:

$$(-2\mu_c K_Y^2) \lambda_c^2 + (C_{m_{\alpha}} + C_{m_q}) \lambda_c + C_{m_{\alpha}} \quad (2.25)$$

Phugoid Motion

With the short period motion assumptions explained in detail and the resulting characteristic polynomials derived, the assumptions required for the phugoid motion may now be discussed. Naturally, the assumptions used for this cannot be the same as for the short period, as the nature of the manoeuvre is different. For the phugoid motion, two sets of assumptions can be made. Unlike in the short period, these two sets are not applied in sequence. Instead, they can be applied independently of each other, leading to slightly different results, each with their own set of benefits and drawbacks (which will be discussed in the Verification section of the report). The first set of potential assumptions is the following: the change in pitching velocity is zero and the angle of attack of the aircraft is zero. The change in pitching velocity is justifiable on the basis that the duration of the motion is very long. As a result, it can be argued that the instantaneous change in the vertical motion of the aircraft must be negligibly small (but doesn't have to be zero). Because of no change in vertical pitch velocity, the equation of the moment M_Y becomes redundant and can therefore be left out of the system matrix (i.e. the bottom row can be removed). The assumption of an angle of attack being equal to zero holds as a consequence of the stability derivative $C_{m_{\alpha}}$ being a highly negative value. As a result, all the coefficients for α in the vector of unknowns are redundant, therefore the second column of the system matrix can be removed. Furthermore, if the angle of attack is zero, then the pitch angle is also equal to zero, leading to a value of C_{X_0} which is also equal to zero. Finally, once again the value of C_{Z_q} is neglected on the basis that the mass parameter is much, much bigger. With these effects highlighted, the system matrix of the original EOM is reduced to the matrix shown below [1]:

$$\begin{bmatrix} C_{X_u} - 2\mu_c D_c & C_{Z_0} & 0 \\ C_{Z_u} & 0 & 2\mu_c \\ 0 & -D_c & 1 \end{bmatrix} \begin{bmatrix} \hat{u} \\ \theta \\ \frac{q\bar{c}}{V} \end{bmatrix} = 0 \quad (2.26)$$

Using this matrix, the coefficients for the characteristic polynomial is shown below [1]:

$$A = -4\mu_c^2$$

$$B = 2\mu_c C_{X_u}$$

$$C = -C_{Z_u} C_{Z_0}$$

The alternative set of assumptions is very similar to the first one; except for the difference that, rather than immediately assuming that the angle of attack is zero, it merely assumes that its variation over time is negligible (i.e. $\dot{\alpha} = 0$). As a result, the coefficients for the alpha unknown cannot be removed from the system matrix like earlier; however, this does continue to lead to significant simplifications nonetheless. Because the variation in the angle of attack is assumed to be very small, the flight path angle must be equal to the pitching angle [1].

$$\begin{bmatrix} C_{X_u} - 2\mu_c D_c & C_{X_\alpha} & C_{Z_0} & 0 \\ C_{Z_u} & C_{Z_\alpha} & 0 & 2\mu_c \\ 0 & 0 & -D_c & 1 \\ C_{m_u} & C_{m_\alpha} & 0 & C_{m_q} \end{bmatrix} \begin{bmatrix} \hat{u} \\ \alpha \\ \theta \\ \frac{q\bar{c}}{V} \end{bmatrix} = 0 \quad (2.27)$$

This leads to the following coefficients of the characteristic equation [1]:

$$\begin{aligned} A &= 2\mu_c(C_{z_\alpha} C_{m_q} - 2\mu_c C_{m_\alpha}) \\ B &= 2\mu_c(C_{X_u} C_{m_\alpha} - C_{m_u} C_{X_\alpha}) + C_{m_q}(C_{Z_u} C_{X_\alpha} - C_{X_u} C_{Z_\alpha}) \\ C &= C_{Z_0}(C_{m_u} C_{Z_\alpha} - C_{Z_u} C_{m_\alpha}) \end{aligned}$$

2.5.2 Asymmetric Motions

The asymmetric eigenmotions are defined by the eigenvalues of the system. To find these, Equation 2.12 should be solved. However, simplifications can be made to simplify the calculations. First of all, C_{Y_β} and C_{n_β} can be neglected. Furthermore, depending on the eigenmotions further simplifications can be made. The motions that will be discussed are the highly damped aperiodic roll motion, the aperiodic spiral motion, and the dutch roll in Subsubsections 2.5.2, 2.5.2, and 2.5.2, respectively.

Highly Damped Aperiodic Roll Motion

The highly damped aperiodic roll motion is caused by a pulse input on the aileron. First of all, by making the assumption that the aircraft only rolls over the longitudinal axis, the aperiodic motion can be approximated. This is a valid assumption, since the aperiodic motion is most of the time damped before other eigenmotions of the aircraft start. The effect of this assumption is that the angle of side-slip β and the non-dimensional yaw rate $\frac{rb}{2V}$ are removed. Moreover, also the lateral force equation and the yawing moment equation can be omitted, leaving only the rolling moments and angle of roll ϕ equations. However, the kinematic relation becomes redundant and can therefore be removed as well, leaving Equation 2.28 [1].

$$(C_{l_p} - 4\mu_b K_X^2 D_b) \frac{pb}{2V} = 0 \quad (2.28)$$

From Equation 2.28, the corresponding eigenvalue for the eigenmotion can now easily be derived by solving Equation 2.29 [1].

$$\lambda_{b_1} = \frac{C_{l_p}}{4\mu_b K_X^2} \quad (2.29)$$

Aperiodic Spiral Motion

The aperiodic spiral motion is a motion in which the aircraft sideslips, yaws and rolls. Furthermore, this motion is generally very slow, which leads to the assumption that all linear and angular accelerations can be neglected, meaning that [1]

$$D_b \beta = D_b \frac{pb}{2V} = D_b \frac{rb}{2V} = 0$$

Furthermore, C_{Y_r} can be omitted, since it is a lot smaller than μ_b . Moreover, also C_{Y_p} can be neglected since it is almost zero. This leads to the final system of aperiodic equations of motion given in Equation 2.30 [1].

$$\begin{bmatrix} C_{Y_\beta} & C_L & 0 & -4\mu_b \\ 0 & \frac{-1}{2}D_b & 1 & 0 \\ C_{l_\beta} & 0 & C_{l_p} & C_{l_r} \\ C_{n_\beta} & 0 & C_{n_p} & C_{n_r} \end{bmatrix} \begin{bmatrix} \beta \\ \phi \\ \frac{pb}{2V} \\ \frac{rb}{2V} \end{bmatrix} = 0 \quad (2.30)$$

Now, by setting the determinant of the characteristic matrix, the according eigenvalue for this eigenmotion can be found from solving Equation 2.31 [1].

$$\lambda_{b_4} = \frac{2C_L(C_{l_\beta}C_{n_r} - C_{n_\beta}C_{l_r})}{C_{l_r}(C_{Y_\beta}C_{n_r} + 4\mu_bC_{n_\beta}) - C_{n_p}(C_{Y_\beta}C_{l_r} + 4\mu_bC_{l_\beta})} \quad (2.31)$$

To have a stable motion, meaning that the motion converges, $\lambda_{b_4} < 0$ should be satisfied. In case all stability derivatives have their normal signs the denominator is negative, this means that [1]

$$C_L(C_{l_\beta}C_{n_r} - C_{n_\beta}C_{l_r}) > 0$$

Dutch Roll (Including the Rolling Motion)

Since during the flight both a yaw and roll motion were observed, the rolling motion cannot be neglected to simplify the equations of motions for the Dutch roll. However, it will be assumed that the centre of gravity moves on a straight line. This assumption is valid since the change in course during the flight due to this motion was very small, and therefore negligible. This leads to a constant course angle, χ , with $\chi = \beta + \psi = 0$, which leads to $\beta = -\psi$. This suggests that the Y-equation is redundant. Moreover, the remaining equations can be simplified by using the fact that $\frac{r_b}{2V} = \frac{1}{2}D_b\psi$ and $\beta = -\psi$. From this, Equation 2.32 was obtained [1].

$$\begin{bmatrix} -C_{l_\beta} + \frac{1}{2}C_{l_r}D_b + 2\mu_bK_{XZ}D_b^2 & C_{l_p} - 4\mu_bK_X^2D_b \\ -C_{n_\beta} + \frac{1}{2}C_{n_r}D_b - 2\mu_bK_Z^2D_b^2 & C_{n_p} + 4\mu_bK_{XZ}D_b \end{bmatrix} \begin{bmatrix} \psi \\ \frac{pb}{2V} \end{bmatrix} = 0 \quad (2.32)$$

Now, the characteristic equation from this system is of the form [1],

$$A\lambda_b^3 + B\lambda_b^2 + C\lambda_b + D = 0$$

with,

$$\begin{aligned} A &= 4\mu_b^2(K_X^2K_Z^2 - K_{XZ}^2) \\ B &= -\mu_b\{(C_{l_p} + C_{n_p})K_{XZ} + C_{n_r}K_X^2 + C_{l_p}K_Z^2\} \\ C &= 2\mu_b(C_{l_\beta}K_{XZ} + C_{n_\beta}K_X^2 + \frac{1}{4}(C_{l_p}C_{n_r} - C_{n_p}C_{l_r})) \\ D &= \frac{1}{2}(C_{l_\beta}C_{n_p} - C_{n_\beta}C_{l_p}) \end{aligned}$$

2.6 Simulation *Lorenz*

The simulation designed in this work aims to predict the response of an aircraft initially in stationary symmetric horizontal flight to inputs in the elevator, the rudder or the aileron control surface, based on stability derivatives and some stationary measurements. A Cessna Citation II was used to obtain such stationary measurements and validate the simulation, additionally the aircraft stability derivatives derived in previous work were provided by [4].

First, the inputs of the numerical model are processed and made compatible with the Python V3 environment used. The data was divided in five dictionaries: HandData, containing the stationary measurements taken manually by the team during the flight test; variables_dict, putting together all the stability derivative values as well as information about the aircraft configuration (the Cit_par22 data) given by [4]; dict_CG, collecting the information about the mass and centre of gravity of the aircraft; dictFT, containing the raw flight data recorded at 10 Hz; and finally eigMotion, collecting the flight data recordings relative to each eigenmotion separately (each sequenced to only contain the relevant information). While doing so, all data (except the dict_CG information) was converted to SI units. Additionally, the flight data for each eigenmotion is non-dimensionalised such that it can be compared to the simulation output.

Based on the recorded fuel flow data during the flight, as well as the information about the centre of gravity calculation given by [4], the variation in mass and centre of gravity location of the aircraft was computed. The mass of the aircraft at all times is extremely important for both the processing of the stationary measurements and the simulation of the aircraft response, as some stability coefficients are weight-dependent.

Following, the stationary measurements taken by the team during the flight were processed in order to obtain the lift-drag polar and the reduced elevator trim and control force curves of the Cessna Citation II. To do so, the thrust at all measurement points was computed using the Excel Sheet provided by [5]. This must be done manually for each new set of data points, however, the simulation outputs a csv containing all the required inputs such that this can be done smoothly

and with little risk for errors. Furthermore, the difference between the real and standard thrust, ΔT , is also output by the Excel Sheet (added feature by the team) and is also to be added for each new data set. Having added this data (the former to the HandData dictionary, the latter directly in main.py), the ΔT is non-dimensionalised for further computations.

Continuing, the lift-drag polar as well as the $C_L - \alpha$ and $C_D - \alpha$ curves of the aircraft are obtained by considering the first set of stationary measurements under the assumptions of steady horizontal symmetric flight ($L = W$ and $D = T$) and by determining the true airspeed. Therefrom, the zero lift drag coefficient C_{D_0} , the Oswald efficiency factor e , the slope of the lift curve C_{L_α} and the zero lift angle of attack (AoA) α_0 are derived using linear regression on appropriate graphs. Furthermore, the elevator effectiveness C_{m_δ} is determined using two data points of the stationary measurements between which a shift in centre of gravity of the aircraft was caused by a passenger going from the back to the front of the vehicle. The C_{m_α} coefficient was then found from the measured elevator trim curve and the previously determined C_{m_δ} coefficient. The reduced elevator trim and control force curves were then obtained by reducing the measured data points as described in [4], those curves are used to analyse and confirm the static stability of the aircraft.

All the previously determined data is then fed into the state space system described in Section 2.3 for both the symmetrical and asymmetrical case. The state space system is set up for each manoeuvre using the state variables of the vehicle at the start of the manoeuvre, and the behaviour of the system with respect to the control surface inputs recorded during the flight is simulated using the Python Control Package and its forced_response function. The system response is then plotted with the actual recorded non-dimensionalised flight data such that validation of the model can be performed.

A complete overview of the code is furthermore given by Figure 2.3.

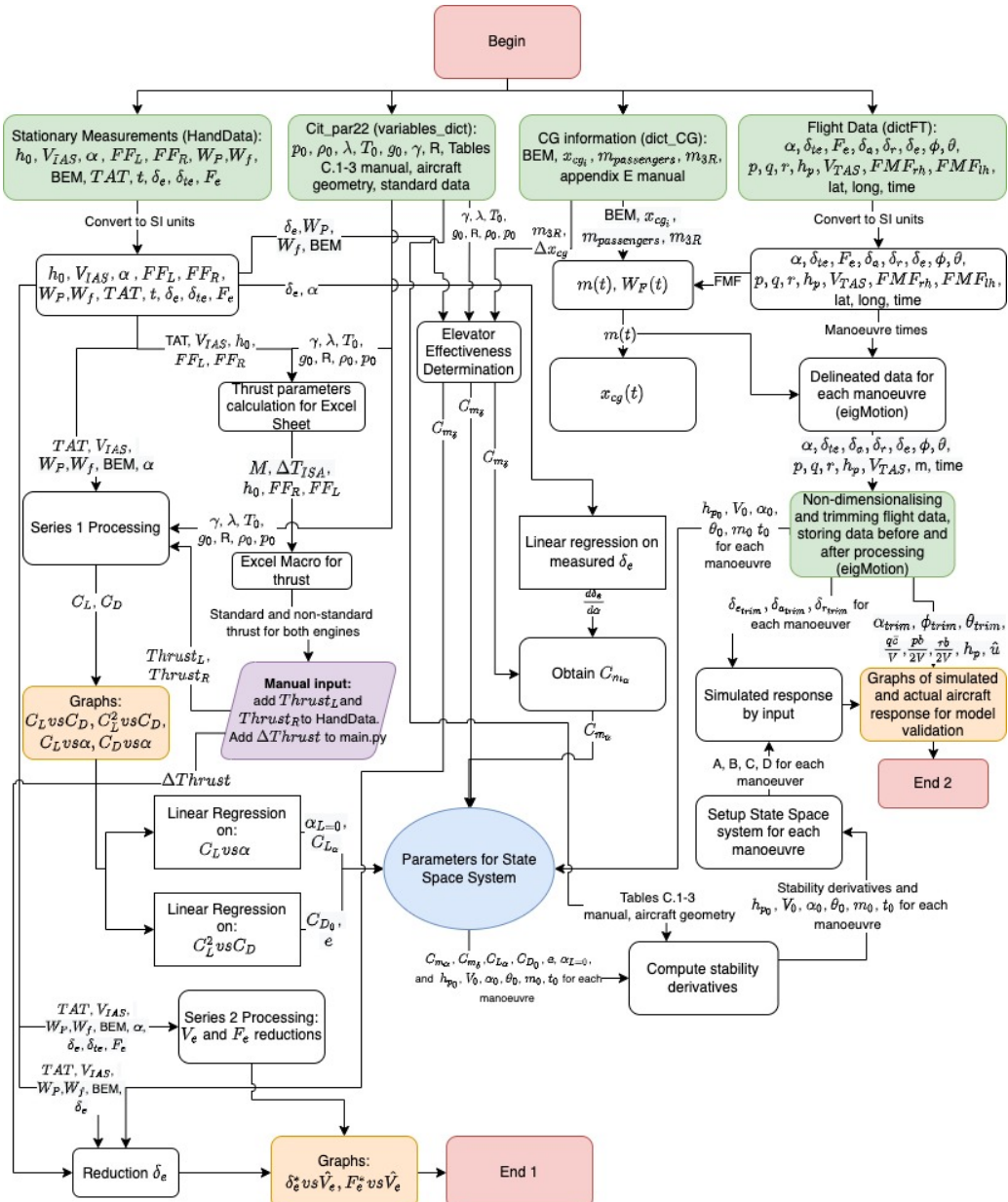


Figure 2.3: Numerical Model Flow Chart

Flight Data Processing 3

In this chapter, the data obtained during the flight test is processed, and key stability parameters are obtained. Those determined parameters will then be fed into the simulation presented in Section 2. First, an overview of the flight will be presented in Section 3.1. This will be followed by the mass and balance overview, given in Section 3.2. Then, the lift-drag polars, resulting from the stationary measurements, are presented in Section 3.3 followed by the elevator trim curve measurements in Section 3.4. Finally, the dynamic measurements will be presented in Section 3.5.

The variables are separated into three categories:

- **Controllable** - can be adjusted in flight to any predetermined (i.e. change in airspeed by changing power)
- **Adjustable** - can be adjusted in flight but not to a predetermined value, its value can be taken into account by considering proper measures like estimating fuel consumption and carrying enough fuel prior to take-off (i.e. the current aircraft mass before measurements changing due to fuel burnt)
- **Uncontrollable** - not normally controllable during flight (i.e. the outside air temperature)

3.1 Flight Overview Niek

In this section, an overview of the flight will be presented. This overview will consist of both weather conditions and the different flight (and measurement) stages. The test flight was scheduled on March 4th 2022 between 14:00 and 15:15. It was 11°C with clear blue skies, which resulted in optimal flight conditions with minimal turbulence. During the flight, two colliding air layers were encountered, which resulted in a small bit of turbulence. However, the hand measurements were not taken during this encounter, thus having no effect on the collected data.

The data acquired during the flight can be split into three parts:

- **First Series Static Measurements.** In the first part, measurements of h , V_{IAS} , α , TAT , fuel flow of both engines and the weight of the fuel consumed at a certain time of flight. The measurements were repeated by each student and then averaged out before processing.
- **Second Series Static Measurements.** In the second part of the flight, measurements were made of h , V_{IAS} , α , TAT , F_e , δ_e and the fuel flow of both engines. For the last measurement series, centre of gravity of the aircraft was shifted. The measurements were split up between the 3 groups of students. The aircraft was also stationary during those measurements. Once the data was averaged out, it was used to process and analyse elevator trim curve plots.
- **Dynamic Manoeuvres.** In the last part of the flight, several eigenmotion manoeuvres were performed to demonstrate the stick-free stability of the aircraft.

3.2 Mass and Balance Julie, Niek

In this section, the mass of the aircraft as a function of time as well as the centre of gravity shift during the flight is analysed.

3.2.1 Change of Total Aircraft Mass over Time

The mass of the aircraft can be divided in three parts: the Basic Empty Mass (BEM), fuel mass and payload mass. An overview of these masses are given in Figure 3.1. The mass changes during the flight due to fuel being burned. The fuel flow, measured every 0.1 seconds (10 Hz), was averaged to a fuel flow for every second. The fuel flow was then subtracted from the total ramp mass, resulting in Figure 3.2.

Table E.1. Citation II

Mass and Balance form

payload computations				mass and balance computations		
crew and pax	$x_{cg,datum}$ [inches]	mass [pounds]	moment [inch-pound]	item	mass [pound]	moment [inch-pounds]
seat 1	131	229.3	30035.8	basic empty mass		
seat 2	131	205.0	26858.9	$x_{cg,datum}$ at BEM = 291.7	9165	2672972.3
seat 3	214	156.5	33497.1			
seat 4	214	119.0	25476.6	Payload		
seat 5	251	165.3	41502.0			
seat 6	251	158.7	39842.0	zero fuel mass		
seat 7	288	172.0	49524.7	at ZFM = 280.0	10699.4	2996104.1
seat 8	288	174.2	50159.5			
seat 10	170	154.3	26235.0	fuel load		
<i>baggage</i>						
Nose	74	0	0	ramp mass		
aft cabin	321	0	0	$x_{cg,datum}$ at RM = 281.5	14749.4	4152289.1
	338	0	0			
				Note: a heavy line above a field means that the preceding fields have to be summed.		
payload		1534.4	323131.8			

Figure 3.1: Mass and Balance Sheet

3.2.2 Change in the Center of Gravity over Time

In this subsection, the change of the centre of gravity over time and the shift in centre of gravity due to the change of position of one of the passengers are presented.

The change in the centre of gravity over time described as a percentage of the mean aerodynamic chord is presented in Figure 3.3. This was calculated by summing the moments due to the mass of the payload, the fuel and the empty aircraft with respect to the chosen datum, which was taken as the nose of the aircraft in this case, after which it was divided by the total mass of the aircraft for the specified time. Furthermore, the change in centre of gravity is due to the fact that fuel is burned, which changes the moment arm due to the fuel. However, it can be concluded that the change due to the burning of fuel is almost negligible.

Finally, we can also look at the shift of the centre of gravity location due to a passenger changing its location. More specifically, the person sitting at seat 8, located at 251 inches from the datum, moved to seat 9, located at 170 inches from the datum. As can be seen from Figure 3.4 this resulted in a 0.017% change in the x_{cg}/MAC position, which corresponds to a shift of 0.035m.

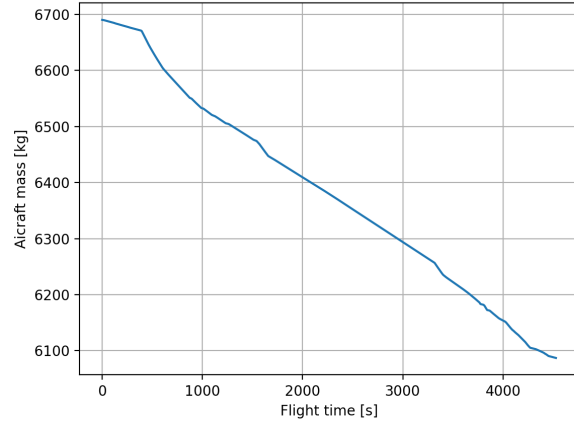


Figure 3.2: Change of Total Mass during flight

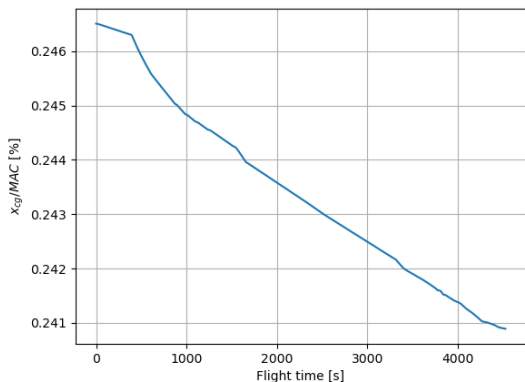


Figure 3.3: Location Change of the Center of Gravity over Time due to the Burning of Fuel

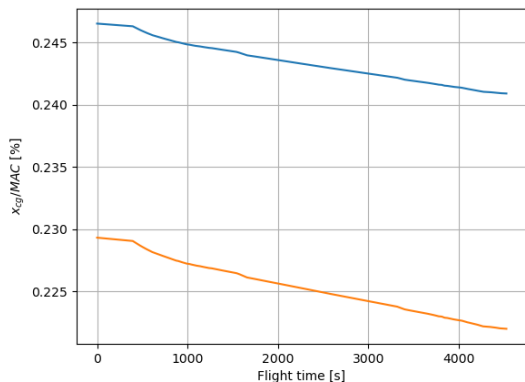


Figure 3.4: Location Change of the Center of Gravity over Time due to Passenger Changing Position

3.3 Lift-Drag Polar *Lorenz, Joao*

The first series of measurements aimed at investigating the lift-drag polar of the Cessna Citation II used for the flight test. Namely, the zero-lift drag coefficient CD_0 , the Oswald efficiency factor e , the zero-lift angle of attack α_0 and the slope of the $C_L - \alpha$ curve $C_{L\alpha}$. Those aerodynamic parameters will then be fed to the numerical model in order to simulate the dynamic behaviour of the aircraft. Table 3.1 gives the data that was obtained through averaging the hand measurements made by all team members during the flight.

Table 3.1: First series of stationary measurements of the flight test

Set number	h [ft]	V_{IAS} [kts]	α [deg]	FFI [lbs/hr]	FFr [lbs/hr]	W_f [lbs]	TAT [$^{\circ}C$]
Static 1	5000	248.000	1.733	750.667	796.333	298.667	10.4
Static 2	4997	222.500	2.450	579.833	606.667	340.000	8.0
Static 3	4995	191.667	3.567	508.167	556.167	369.833	6.4
Static 4	5000	161.833	5.333	472.833	505.667	403.000	4.1
Static 5	4990	132.667	8.650	419.333	463.167	423.167	3.5
Static 6	5010	118.667	10.65	445.000	485.667	462.667	3.0

Note that the first step was to convert all those values to SI units. As described in Section 3.1 the two first measurement series were made in horizontal, stationary and horizontal flight, meaning that for the purpose of the lift-drag polar generation: $L = W$ and $D = T$. The overall workflow is presented in the following:

1. Because the weight is an adjustable variable, as explained in the Chapter introduction, all measurement point were obtained using W_f and the take-off weight W_{to} : $W = W_{to} - W_f$. This weight is taken as the lift generated by the main wing during this flight configuration at the time of the measurement. That is, the contribution to the lift from the horizontal stabilizer is neglected.
2. The equivalent airspeed is obtained by following the method presented in [4, p.9]. This airspeed permits to compute the dynamic pressure as $\frac{1}{2}\rho_0 V_e^2$.
3. The lift coefficient for all six data points is then computed using $C_L = \frac{2W}{\rho_0 V_e^2 S}$.
4. The thrust force was obtained using the macros from [5], requiring the altitude, the Mach number, temperature difference with respect to International Standard Atmosphere (ISA) and the fuel flow in both engines. Having computed the thrust force, the drag force was obtained $D = T = T_R + T_L$.
5. The drag coefficient is then obtained similarly to the lift coefficient $C_D = \frac{2T}{\rho_0 V_e^2 S}$.

From this workflow, the plots shown in Figures 3.5a-3.5d were obtained. As a sanity check, the fitted plots were visually inspected to ensure a proper fit with respect to the theory. The results were compared with trustworthy literature [6] [7] to make sure the measured date would follow the correct trend.

Using Figure 3.5a, the aerodynamic parameters CD_0 and e can be obtained through a linear regression on C_D and C_L^2 ($y = m \cdot x + c$) and analysing the obtained relation. Theoretically, the drag coefficient can be approximated from $C_D = CD_0 + \frac{C_L^2}{\pi A e}$, meaning that the linear regression coefficients are related to the aerodynamic parameters by: $CD_0 = c$ and $e = \frac{1}{mA\pi}$. Similarly, α_0 and $C_{L\alpha}$ can be obtained from Figure 3.5b, using a linear regression ($y = m \cdot x + c$): $C_{L\alpha} = m$ and $\alpha_0 = -c/m$. Table 3.2 gives the obtained parameters for both the flight test and the *data_ref_2022*.

Table 3.2: Primary aerodynamic parameter for both the flight test and *data_ref_2022*

Parameter	B15	Reference
CD_0 [-]	0.0195	0.0225
e [-]	0.7810	0.8221
$C_{L\alpha}$ [1/rad]	4.7166	4.5380
α_0 [deg]	-0.8898	-1.0512

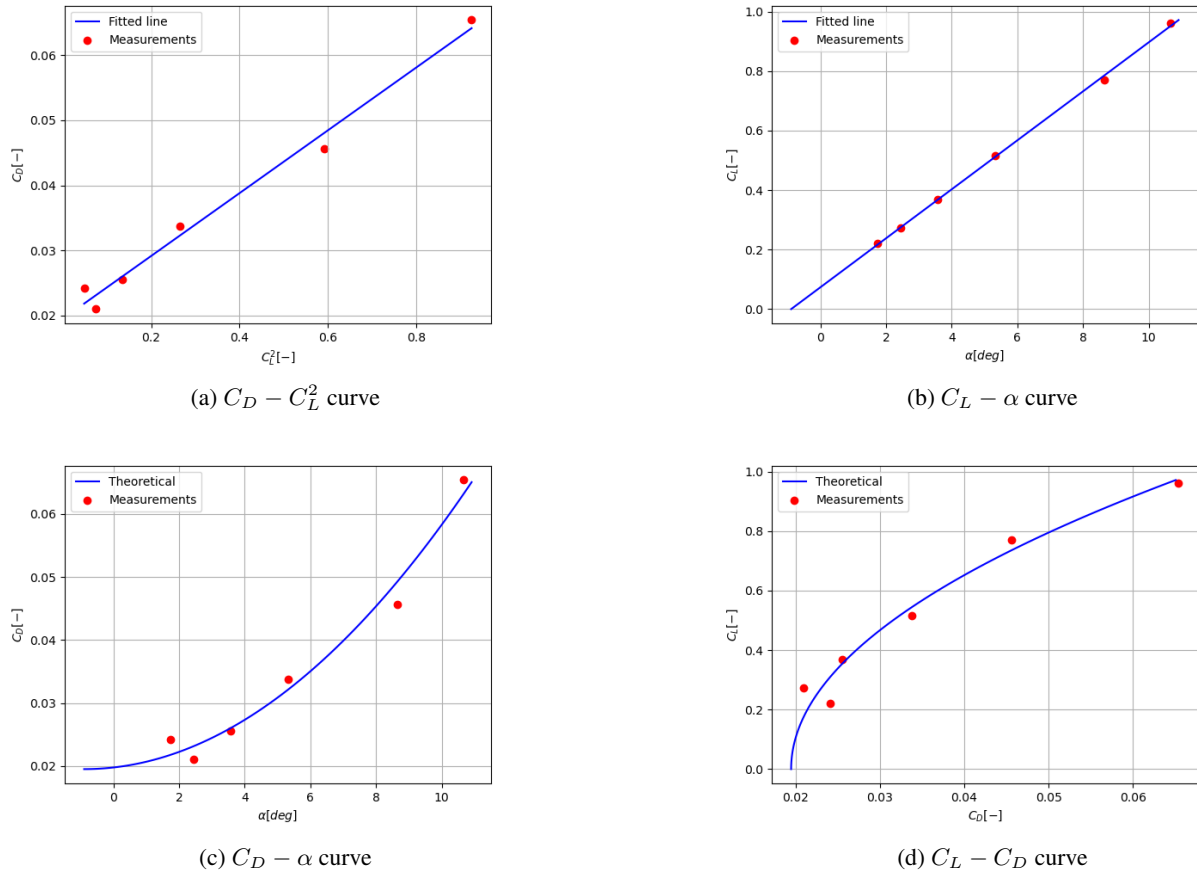


Figure 3.5: Lift-Drag measurements for series 1

3.4 Elevator Trim Curve Static Measurements_{Joaoo}

In this section, plots and calculations related to the second part of the static measurements will be performed. These are associated to the elevator trim curve. The first Subsection, 3.4.1, shows the parameters and calculations required to obtain $C_{m\delta}$. Next, Subsection 3.4.2 explains how $C_{m\alpha}$ was obtained by the means of the static measurements data. Then, in Subsection 3.4.3, it is explained how the engines thrust were obtained and later non-dimentionalised to be used to reduce some parameters. Finally, Subsection 3.4.4 shows plots for the reduced elevator deflection and reduced stick force against reduced equivalent airspeed. An overview of all static measurements taken during the flight by the team and later averaged are displayed on Table 3.3. Note that the last two rows were not used for the plot since the aircraft was again trimmed at measurement 8, seen by the zero stick Force, and the cg was later shifted by a moving passenger on measurement 9. Hence, these last entries were not used for the plots in Subsection 3.4.4.

Table 3.3: Second series of stationary measurements of the flight test

Set number	h [ft]	V_{IAS} [kts]	α [deg]	FFI [lb/hr]	FFr [lbs/hr]	Wf [lb]	TAT [$^{\circ}$ C]	δ_e [deg]	Fe [N]
Elevator 1	6960	160.000	5.600	431.0	462.0	567.0	1.2	0.1	0.0
Elevator 2	7068	151.000	6.283	429.0	460.0	588.5	0.65	-0.3	-18.0
Elevator 3	7248	138.333	7.633	423.0	455.5	615.5	0.2	-0.9	-30
Elevator 4	7442	131.000	8.733	423.0	451.5	646.0	-1.0	-1.3	-34.0
Elevator 5	6452	170.667	4.717	438.0	470.5	687.0	3.5	0.45	19.7
Elevator 6	6060	179.500	4.117	445.0	476.0	710.0	4.2	0.7	37.0
Elevator 7	5458	189.000	3.617	456.0	486.5	734.5	5.5	0.9	53.0
Elevator 8	5812	161.500	5.383	447.0	478.0	758.0	2.8	0.15	0.0
Elevator 9	5824	161.800	5.380	447.5	478.5	788.0	2.8	-0.3	-20

3.4.1 Moment Coefficient due to Elevator C_{m_δ}

For future computations of elevator deflection, the moment coefficient due to the elevator must be known. This will be performed and explained in this section. Equation 3.3 illustrates the necessary variables to calculate C_{m_δ} . A few parameters present in Equation 3.3 are already known, either from the performed measurements during the flight test or given by the assignment such as aircraft configuration properties, namely the chord. Some other parameters, however, remain unknown or have not been processed yet, such as C_N and Δx_{cg} .

For the calculation of Δx_{cg} a simple algebraic expression was used, presented in Equation 3.1, to determine the change in centre of gravity along the x-axis. The parameters required to compute this are, the mass of the passenger on seat 8, the x coordinate change from position 10 to 8, and the current mass of the system. All these parameters are given on Figure 3.1 except for the current mass, this was computed by subtracting the fuel consumption, obtained by averaging the fuel consumption right before and right after the static measurement when passenger 8 moved, from the mass at EOBT of the aircraft. Using the method described, a value for the change in centre of gravity was calculated to be: $\Delta x_{cg} = -0.0354 \text{ m}$

Similarly, for the calculation of C_N given by Equation 3.2, some parameters are given or known, namely S and ρ_0 . The rest of the parameters need to be determined, namely the equivalent airspeed, atmospheric density at current flight level and the current weight. This can be easily obtained by multiplying the current mass by the acceleration due to gravity. The equivalent airspeed is obtained by reducing the calibrated airspeed to equivalent airspeed as explained previously in section 3.3. The conversion from indicated to calibrated airspeed is a simple relation given by the assignment: $V_{CAS} = V_{IAS} - 2 [\text{kts}]$. Using this method, a result for the normal coefficient is computed to be $C_N = 0.53013$.

$$\Delta x_{cg} = \frac{m_8 \cdot (x_{10} - x_8)}{m_{current}} \quad (3.1)$$

$$C_N = \frac{W_{current}}{\frac{1}{2} \rho_0 V_e^2 S} \quad (3.2)$$

$$C_{m_\delta} = -\frac{1}{\Delta \delta_e} \cdot C_N \cdot \frac{\Delta x_{cg}}{c} \quad (3.3)$$

Using the parameters computed above to calculate C_{m_δ} from the Equation 3.3 the numerical value of $C_{m_\delta} = -1.1614$ is found. The value computed for the reference data is shown below on Table 3.5.

Table 3.4: Comparison with *data_ref_2022*

	B15	Reference
C_{m_δ}	-1.16142	-1.29881

3.4.2 Longitudinal Stability Coefficient C_{m_α}

For the C_{m_α} calculation, a simple expression is used, namely Equation 3.4. Two parameters are needed and one of them was already computed, as shown in subsection 3.4.1. For the determination of $-\frac{d\delta_e}{d\alpha}$ an elevator deflection against angle of attack scatter plot was performed for the stationary measurements, indicated by the red points on Figure 3.6. Subsequently, a least square line was fitted for these data points, illustrated in Figure 3.6 by the blue line. The equation of this line is also shown on the bottom right where the desired parameter can be seen, $\frac{d\delta_e}{d\alpha} = -0.4406$. Using the previously computed value of $C_{m_\delta} = -1.1614$ a value of $C_{m_\alpha} = -0.5036$ is found. This value is shown alongside the reference data value on Table 3.4.

$$C_{m_\alpha} = -\frac{d\delta_e}{d\alpha} \cdot C_{m_\delta} \quad (3.4)$$

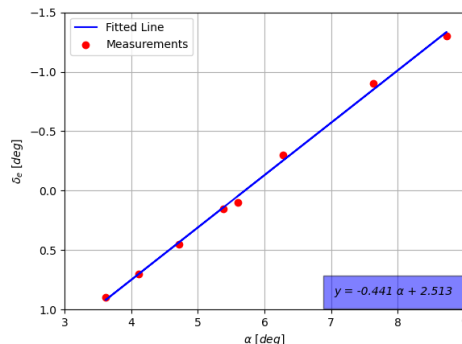


Figure 3.6: Elevator deflection measurements against theoretical computations

Table 3.5: Comparison with *data_ref_2022*

	B15	Reference
C_{m_α}	-0.50357	-0.56434

3.4.3 Dimensionless Standard Thrust Coefficient T_{cs}

As a part of the parameter reduction of certain variables, it is required to reduce the thrust first. This is achieved by the reduction expression presented on Equation 3.5, where T_s is the standard thrust and T is the actual thrust. Both thrust calculations are obtained by making use of an Excel macro provided on Brightspace the sole difference is that for the standard thrust it is assumed that there is no difference between the actual atmospheric temperature and ISA temperature. Once this is performed, the difference between these parameters is taken and then non-dimensionalised by diving the result by $\rho_0 V_e^2 D^2$. The result for each measurement is shown on Table 3.6.

$$\frac{T_s - T}{\rho_0 V_e^2 D^2} \quad (3.5)$$

Table 3.6: Thrust calculations for each series 2 measurements

Measurement	T - Thrust [N]	T_s - Standard Thrust [N]	$\Delta T = T_s - T$	$\Delta T_c = \frac{\Delta T}{\rho_0 V_e^2 D^2}$
1	3762.67	3716.08	-46.60	-0.01228
2	3841.56	3794.46	-47.10	-0.01396
3	3917.25	3873.64	-43.60	-0.01543
4	3995.63	3947.19	-48.43	-0.01913
5	3702.09	3664.77	-37.33	-0.00864
6	3666.92	3623.71	-43.21	-0.00903
7	3664.96	3617.77	-47.19	-0.00888

3.4.4 Reduced Elevator Deflection ($\delta_{e_{eq}}^*$) and Reduced Stick Force (F_e^*)

In this Subsection, a plot of the reduced stick force and elevator deflection against reduced equivalent airspeed is presented. These plots are of great importance because it allows for the comparison with other flight data, due to the reduced parameters, and it to verify that the aircraft is indeed stable by verifying that $\frac{d\delta_{e_{eq}}^*}{dV_e} > 0$ implying $C_{m_\alpha} < 0$.

The elevator deflection was reduced according to the expression presented on Equation 3.6. The thrust parameters present in this Equation were introduced in the past section and are displayed in Table 3.6. $C_{m_{T_c}}$ is the dimensionless thrust moment arm and its value of -0.0064 is given on Table C.2 of Appendix C of the assignment [4]. The value of C_{m_δ} was previously explained on subsection 3.4.1 and a value of -1.1614 is used.

The airspeed was reduced by using Equation 3.7. Once the airspeed was converted from calibrated airspeed to equivalent airspeed, as described in section 3.3, this parameter was reduced by multiplying it by a factor of $\sqrt{\frac{W_s}{W}}$, where $W_s = 60500N$ and the weight W varies with time and was calculated for each data point by subtracting the initial weight with the fuel used up until each measurement time. For the reduced stick force a similar approach was taken, and the expression can be seen on Equation 3.8. An overview of the reduced parameters can be found on Table 3.7.

$$\delta_{e_{eq}}^* = \delta_{e_{eq,meas}} - \frac{C_{m_{T_c}}(T_{cs} - T_c)}{C_{m_\delta}} \quad (3.6)$$

$$\tilde{V}_e = V_e \sqrt{\frac{W_s}{W}} \quad (3.7)$$

$$F_{e_{aer}}^* = F_{e_{aer}} \cdot \frac{W_s}{W} \quad (3.8)$$

Table 3.7: Overview of Reduced Variables

Measurement	$\delta_{eq,meas}$ [deg]	δ_{eq}^* [deg]	F_e [N]	F_e^* [N]	V_e [m/s]	\tilde{V}_e [m/s]
1	0.10000	0.10007	0.00	0.00	81.12	79.44
2	-0.30000	-0.29992	-18.00	-17.29	76.51	74.98
3	-0.90000	-0.89991	-30.00	-28.87	70.02	68.69
4	-1.30000	-1.29989	-34.00	-32.79	66.26	65.07
5	0.45000	0.45005	19.67	19.02	86.58	85.15
6	0.70000	0.70005	37.00	35.84	91.11	89.68
7	0.90000	0.90005	53.00	51.43	95.99	94.56

Finally, once all parameters are converted to reduced form, the following plots are obtained. The results suggest that the aircraft is indeed stable, as it can be seen that $\frac{d\delta_{eq}^*}{d\tilde{V}_e} > 0$ from Figure 3.7 (Note that the y-axis is inverted so it goes from positive to negative as you move up the axis). Figure 3.8 also behaves as expected since from the trim point ($F_e = 0$) a decrease in airspeed leads to negative values of F_e suggesting that the pilot needs to pull on the yoke to raise the nose and keep the aircraft levelled at a lower speed. The opposite is also true, leaving from the trim point a higher airspeed suggests pushing on the yoke, shown on the graph by positive values of F_e , to keep the aircraft levelled.

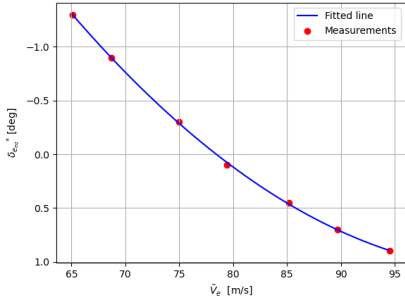


Figure 3.7: Reduced Elevator deflection measurements and fitted line

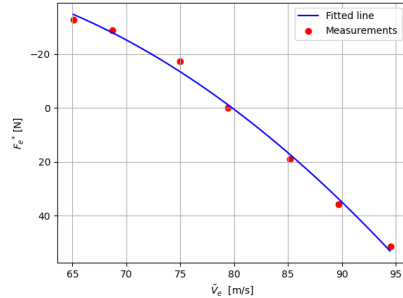


Figure 3.8: Reduced Stick force measurements and fitted line

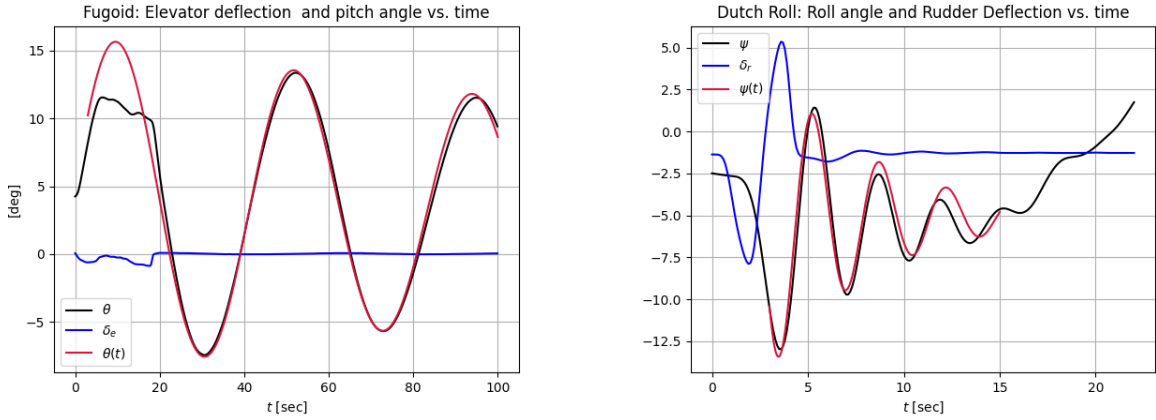
3.5 Dynamic Measurements Processing *Alex*

As part of the flight test, several dynamic manoeuvres have been performed. The relevant measured aircraft state variables, such as pitch angle θ , pitch rate q and other asymmetric motion variables, have been analysed.

3.5.1 Flight Data Analysis

It has been found that the phugoid and Dutch roll eigenmotions show the best match with the underdamped decaying oscillation motion. Unfortunately, the short period eigenmotion was too irregular to properly analyse. Those motions will be plotted in this section and relevant parameters will be calculated. There are a number of analytical techniques to find the damping ratio, period and other characteristics from experimental measurements, but for those two cases a decaying sinusoidal function will be plotted to match the flight data, and those characteristics will then be calculated from the equation of best-fit of the form:

$$\theta(t) = a_0 + A \exp(-\lambda t) \cos(\omega t + \phi) \quad (3.9)$$



$$(a) \phi(t) = 3.49 + 12.7 \exp(-0.0045t) \cos(0.149t - 1.45)$$

$$(b) \psi(t) = -5.03 + 15.9 \exp(-0.183t) \cos(1.8t - 3.2)$$

Figure 3.9: Flight Data for Phugoid and Dutch Roll eigenmotions

The period P for both cases can be calculated easily by $P = \frac{2\pi}{\omega}$. The $T_{1/2}$, time to half-amplitude can also be easily found by $T_{1/2} = \frac{\log(\frac{1}{2})}{\lambda}$, or $T_{1/2}^* = \frac{\log(\frac{1}{2})}{\lambda} \frac{\bar{c}}{V}$ for the non-dimensional time. The damping ratio $\zeta = \frac{\lambda}{\sqrt{\lambda^2 + \omega^2}}$, where the ω is the natural frequency and λ is the decay rate which can be taken from Equation 3.9.

Table 3.8: Eigenmotion characteristics as derived from the flight data

Eigenmotion	P [s]	P^* [-]	$T_{1/2}$ [s]	$T_{1/2}^*$ [-]	ω [rad/s]	ζ [-]	$\frac{\bar{c}(b)}{V}$ [s]
Phugoid	42.2	0.486	154	1.78	0.149	0.03018	0.0116
Dutch Roll	3.49	0.315	3.79	0.342	1.8	0.1011	0.0904

Table 3.9: Eigenmotion characteristics as derived from the reference flight data

Eigenmotion	P [s]	P^* [-]	$T_{1/2}$ [s]	$T_{1/2}^*$ [-]	$\frac{\bar{c}(b)}{V}$ [s]	Equation
Short Period *	29.36	0.348	13.33	0.1582	0.0119	$2.7 + 26.2 \exp(-0.052t) \cos(0.214t - 2.9)$
Phugoid	43.0	0.512	108.3	1.29	0.0119	$3.2 + 10.13 \exp(-0.0064t) \cos(0.146t - 1.6)$
Dutch Roll	3.22	0.300	3.15	0.293	0.0930	$-1.2 + 15.7 \exp(-0.22t) \cos(1.95t - 1)$

* - there has been no short duration motion found during the given time for the short period eigenmotion, so those characteristics are probably not correct. Instead, the results are given for a much prolonged manoeuvre that was found at that timestep, with the decaying sinusoidal motion.

3.5.2 Flight Data Non-Dimensionalisation

The data that has been measured during the test flight has been initially cropped to save relevant state variables for each eigenmotion. The time duration was chosen by waiting for when the eigenmotion is sufficiently decayed or when the pilot has disturbed the control stick. Since the flight data has been originally measured in (partly) imperial units, several steps were taken so that it can be compared to the numerical model. Those conversions, as well as the data processing and cropping have been carried out through Python code, which is accessible on Gitlab. Specifically, first all the data has been converted to SI units for ease of use and to avoid conversion mistakes. Afterwards, the data vectors were trimmed according to the time of eigenmotions, and assembled into a single dictionary structure. Based off that dictionary, which had state measurements in SI units, a new dictionary was created which had non-dimensionalised state measurements. These were then used to create plots which will be compared to the plots made through the use of the simulation.

Verification 4

Verification is a crucial part in the verification and validation process when building a numerical model. More specifically, verification is needed in order to check if the model implementation is accurately representing the conceptual description of the model and its solution [8]. Moreover, verification should be done on different levels. This is done by performing, unit tests, subsystem tests, and system tests. The verification steps for various parts of the code are described in this chapter. Verification of reduction and converter routines is done in Section 4.1, then mass and c.g. calculations are verified in Section 4.2, afterwards data processing as a whole is verified in Section 4.3. Recorded data was verified in section 4.3, and state-space model in Section 4.5. Finally, some global tests were performed in Section 4.6. A reflection on the test accuracy is finally given in Section 4.7.

4.1 Verification of Unit Converters and Reduction of Measured Airspeed *Oliver*

Before verifying the wider simulation and its underlying functions, it is first important to ensure that the measured data from the flight test has been translated to the correct units and have been reduced to standards which conform to the International Standard Atmosphere conventions and to the standard mass of the aircraft. These verification tests are critical, as the successful reduction of parameters is required for the correct construction of the reduced elevator trim and control force curves based on the unique measurement data which was retrieved by the group during the flight test. The verification tests will begin initially with unit tests of the smaller base functions performing the simplest operations (such as unit conversions), and then move on towards the module testing of the more complex functions which incorporate the aforementioned base functions.

A more detailed outline of each conducted test is shown below:

- **UNIT-CONV-001:** To successfully reduce the parameters, first it is important to convert all the data into SI units. This was done with a number of small base functions containing the individual conversions necessary. Unit tests for these are straightforward, as one needs to simply enter a sample data value, and cross-check the output with the official conversion provided by a valuable resource (these are all available on the Internet). This can be streamlined by making use of the `unit_test` library provided in Python. If multiple sources and the code are in agreement, then the tests have been passed. Asides from minor implementation mistakes, these tests were readily passed.
- **UNIT-CONV-002:** Upon converting the functions to SI units, the various measurement data could be reduced to standard ISA conventions and aircraft standard mass. This procedure (as explained in [4]) consists of a number of correction functions, such as the Ram Air Temperature Correction, and the determination of the equivalent airspeed based on the calibrated measurements. These equations were individually implemented, therefore they may be checked by inserting some sample data, and checking with `unit_test` whether the outputted results matched the results computed by hand (as well as internet calculators if they are available). Once again, apart from minor typos, the checks were readily passed.

Having successfully completed the above tests, the following module test shown below was conducted:

- **MOD-CONV-001:** In order to streamline the process of reducing full sets of data and the need to call the individual conversion functions described above, more compact functions were created which performed the complete reduction procedure of the required data parameters. Given that computing the equivalent results by hand is tedious, the outputted results from these compact equations were directly compared to various internet calculators, and the intermediate results were compared to the previously verified individual functions. This module test was passed without mistakes.

Upon the completion of the tests shown above, there is now reasonable model confidence to suggest that the unit converter and parameter functions work as expected. With that in mind, the next steps of the verification process may take place.

4.2 Verification of Mass and Center of Gravity Calculation *Julie,Niek*

With the data now reduced to standard convention and converted to SI units, the next step in the verification process is reviewing if the functions used for determining the mass and centre of gravity of the aircraft are performing as intended. To do this, unit and module tests were implemented, each of which are discussed below and together show that :

- **UNIT-MASS-001:** The first unit test to be performed is to visually check that the mass and centre of gravity datum positions that were used as an input to the code are consistent with the ones presented in the aircraft manual. Subsequently, the vectors used to calculate the moment due to the fuel mass were inspected to make sure there were no errors in the inputs. From this, it was clear no mistakes were made in the implementation of the parameters.
- **UNIT-MASS-002:** With the visual check complete, a unit test was written to check the calculation for the real-time aircraft mass at three different points in time. This was done by comparing the mass calculated by the function *mass_calculation()* to the mass calculated by subtracting the mass of the used fuel from the ramp mass. This showed that the mass calculation was correct and was therefore verified to be a reliable input for the centre of gravity calculation.

Now that the mass calculation is verified, the moments due to the different mass contributions, respectively the mass of the passengers, the basic empty mass of the aircraft, and the fuel mass, were checked with separate unit tests.

- **UNIT-CG-001:** First, the moment contribution due to the passenger masses was verified by comparing the moment computed by the function *center_of_gravity_calculation()* to the completely written out moment calculation. However, to be certain no mistakes were made in the test, print statements were used to be able to compare the unit test input values to the hand calculated values. This showed that there were no mistakes in the moment calculations.
- **UNIT-CG-002:** In a procedure virtually identical to the one above, the calculation of the moment contribution due to the empty mass of the aircraft of the reviewed. From this unit test, it was shown that there were no mistakes in the moment calculation of the aircraft empty mass. Furthermore, again here the moment calculation was also compared to the hand calculated value, to ensure the accuracy of the unit test.
- **UNIT-CG-003:** Finally, similarly to above, the moment contribution due to the aircraft fuel weight was verified and compared to the hand calculated values of the moment. However, contrary to the above two cases, this unit test checks the moment contribution at three different instances in time, as the mass of the fuel is consistently changing throughout the flight. This unit test was successfully passed, and therefore showed no mistakes were made in the fuel moment calculation.
- **MOD-CG-001:** The functions verified above were all used in combination in order to determine the centre of gravity location of the aircraft at different instances of time. Therefore, a module test must be conducted which tests the assembly of these individual functions together to yield the expected result. This was done by first visually checking if the calculated values for the centre of gravity in inches were in the stability region of the Cessna Citation II (C550), which was defined as the region between STA 276.10 and STA 285.80. Figure 3.3 shows that this requirement was met. Only the calculated values now had to be checked for accuracy. This was done by writing a unit test, which checked that the centre of gravity calculated by *center_of_gravity_calculation()* was equal to the written out calculation for the centre of gravity for three point in time. Moreover, to again check that there were also no mistakes in the unit test the outcome was also checked by comparing the values to hand calculated ones, using the mass and balance form, presented in Figure 3.1. All of this showed that *center_of_gravity_calculation()* performs the correct calculations and gives accurate outputs.

4.3 Verification of Data Processing Calculations *Joao*

During the development phase several blocks of code were checked to ensure that the program was indeed outputting the desired results, when unexpected results were returned a deeper analysis would be carried out to spot potential mistakes in the script. This led to the identification of several errors.

4.3.1 Processing of First Stationary Series of Measurements

In this Subsection, the analysis carried out during the plotting routine is presented. Errors found during the development phase are presented below and the performed sanity checks and tests explained.

- **UNIT-FM-001:** Temperature input was given in degrees Celsius instead of kelvin. This was tested while reducing the speed from indicated airspeed to equivalent airspeed, more specifically when computing the Mach number. When negative valued temperatures in Celsius were used the code returned an error. This is expected since a negative argument was given to a square root function. This was fixed by properly converting the temperature from the data file before processing and plotting results and ensuring a consistent use of kelvin throughout the entire program.
- **SAN-FM-001:** As a part of the data processing verification, sanity checks were performed to guarantee that the averaged measured data would follow the predicted trend from literature. As discussed in section 3.3, the plots do in fact follow the expected trend.

4.3.2 Processing of Second Stationary Series of Measurements

In this Subsection, the analysis carried out during the plotting routine and the errors spotted are presented. A list of errors found during this phase of development is listed below and the performed sanity checks explained.

- **SAN-SM-001:** Missing conversion from degree to radians for $\Delta\delta_e$. When performing sanity checks for the calculations of C_{m_δ} , the numerical result was compared to the reference value given in Table C.2 of Appendix C of the assignment [4]. The numerical value was way off. When tracing back parameters, it was found that the input $\Delta\delta_e$ was given in degrees from the measurement data and a conversion to radians was missing. This was fixed by converting the change in elevator deflection from degrees to radians before calculating C_{m_δ} .
- **SAN-SM-002:** Indicated airspeed was used instead of equivalent airspeed. Similarly to the test above, when comparing C_{m_δ} to the reference data, the result was slightly off. Tracing back the parameters, it was found that V_{IAS} was being used instead of the equivalent airspeed V_e . This was implemented so that the code would use V_e for C_{m_δ} calculations and the final result was much closer to the reference data.
- **SAN-SM-003:** $W_s \neq W_{to}$. The incorrect standard aircraft mass was being used when reducing parameters for the elevator deflection plots. A value of $W_{to} = 6690.223$ N was being used instead of $W_s = 60500$ N. The difference in the output was minimal but nonetheless incorrect, this would lead to future problems when calculating with the reference data since the results would not be quite as expected since a different reference weight was used.
- **SAN-SM-004:** Conversion from lbs to kg of W_f for the elevator trim curve stationary data incorrectly performed. W_f was being converted using conversion functions from *ParameterReduction.py*. The function *lbshtr_to_kgs(x)* was used when the original unit was in fact in pounds, so the correct function to be used would have been *lbs_to_kg(x)*. This was a continuation mistake, since the previous two parameters were indeed in that unit (FFl [lbs/hr] and FFr [lbs/hr]) and required that conversion function to be used. This was adjusted accordingly to ensure a correct unit conversion for both series of stationary measurements.
- **SAN-SM-005:** W_{ac} in kg instead of N. Incorrect unit for the current aircraft weight. Because the weight calculations were in fact performed in units of mass due to the nature of the data given (W_f was given in units of mass not weight) the current aircraft mass was also being used in kg when computations were being performed. This led to mixing up units (W_s in N and W_{ac} in kg) and clearly incorrect results. This was fixed by converting from mass unit to weight unit at the end of the current aircraft mass computations.

4.4 Verification of Recorded Data *Lorenz*

The recorded data received by the team after the flight was then considered carefully to make sure that no error was made in the data acquisition. More specifically, the behaviour of the aircraft with respect to certain inputs are considered, knowing that the aircraft is statically stable.

- **UNIT-REC-001:** the aircraft response to a negative elevator deflection should be a positive pitch angle [1]. The recorded flight data was visually checked to make sure that was the case. As can be seen in Figure 4.1, this is indeed the case on the short run (as expected) and therefore no sign error was found in the recorded elevator input.
- **UNIT-REC-002:** the aircraft response to a positive rudder deflection should be a negative roll angle in the short term [1]. Figure 4.2 was visually checked and clearly the sign of the rudder input was wrongly recorded. This was corrected, and the problem was resolved.

- UNIT-REC-003:** the aircraft response to a positive aileron deflection should be a negative change in the roll angle in the short term [1]. Similarly to the two previous unit tests, Figure 4.3 was visually checked, and clearly this is not the case. This means that the aileron input was probably recorded wrongly, and the sign was switched. This was fixed, and the problem was resolved.

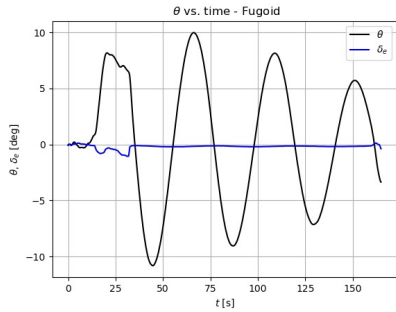


Figure 4.1: Aircraft response to elevator deflection

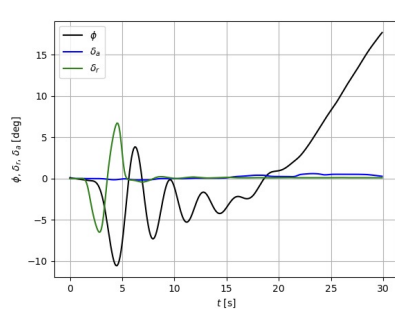


Figure 4.2: Aircraft response to rudder deflection

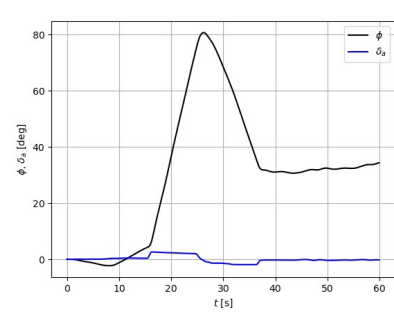


Figure 4.3: Aircraft response to aileron deflection

4.5 Verification of State Space Model and Simplified Eigenmotions *Julie, Oliver, Niek*

Now that it is clear the data processing was carried out correctly, the implemented state space model and its outputs can be verified. The unit and module tests for the verification of the state space model will be presented in this section.

To verify the state space model, the tests identified below were performed in sequence:

- UNIT-STATE-001:** First, the matrices used as inputs to the state space model were visually checked to ensure that the coefficients and the dimensions matched the theoretical expressions. This was done to make sure no mistakes were made in the implementation of the matrices. Upon visual inspection, this test was passed.
- UNIT-STATE-002:** With the state space model correctly set-up, the sign of the real component of the outputted eigenvalues were visually checked, by printing them in the programme. From theory and the known stability properties of the aircraft, it was expected that all eigenvalues apart from the one corresponding to the asymmetric spiral (as this eigenmotion is unstable for the Cessna Citation II (C550)) eigenmotion should be negative. However, this was not the case, as the real parts of the symmetric eigenvalues were found to be positive. It was found that these deviations were due to the fact that the inputs were being updated incorrectly. Upon correcting the inputs, the outputted eigenvalues were of the correct sign.
- MOD-STATE-001:** With the signs of the eigenvalues successfully verified, the values of the eigenvalues calculated by the state space model were verified by comparing them to the eigenvalues computed by solving the characteristic equation for the equations of motion. Moreover, also the implemented characteristic equations, were thoroughly checked in order to avoid mistakes in their implementation in the code. Moreover, the eigenvalues of the state space model were also compared to the eigenvalues of the reference flight data. The results of this are presented in Table 4.1. It can be seen that when comparing eigenvalues of the state space model and the characteristic equation, the values for the symmetric eigenvalues were very close, except for some small deviations. These deviations are due to the fact that in the characteristic equation C_{X_q} , is assumed to be zero. Furthermore, the values of the asymmetric eigenvalues are exactly the same. Therefore, the magnitude of the deviations were deemed to be acceptable, and the test was passed.

Table 4.1: Eigenvalues retrieved from the state space model and the characteristic equation for both symmetric and asymmetric equations of motion

Eigenvalues	State Space Model	Characteristic Equation	Reference Data
Symmetric	$-0.03034661 \pm 0.04241194j$	$-0.03034836 \pm 0.04240892j$	$-0.03078848 \pm 0.04518999j$
	$-0.00010336 \pm 0.00312557j$	$-0.00010191 \pm 0.00312571j$	$-0.00012044 \pm 0.00317655j$
	-0.74903007	-0.74903007	-0.76022692
Asymmetric	$-0.05317902 \pm 0.36764768j$	$-0.05317902 \pm 0.36764768j$	$-0.05406306 \pm 0.37072468j$
	0.00193227	0.00193227	0.0024589

In connection to the state space model which was verified above, it was explained in great detail in section 2.5 that there is a possibility to simplify the Equations of Motion such that they can be solved without numerical software. This, however,

allows for a second module test that checks if eigenvalues of the state space model are correctly computed. This can be done since the analytically computed eigenvalues of the simplified Equations of Motion are expected to be close to the ones calculated by the solving the non-simplified EoM, looking at the results for the Cessna Citation I provided in [1].

- **MOD-STATE-002:** The eigenvalues and the corresponding eigenmotions of the complete system and the simplified systems were represented graphically for both the symmetric and asymmetric motions, shown in Figure 4.4 and Figure 4.5. This was done to help visualize how the values differed in the complex plane between the different assumption cases, and how this in turn impacted the response of the aircraft's dynamic response. Moreover, for the symmetric eigenmotions additional graphical representations for the different sets of assumptions were generated, which are displayed in Figure 4.6 and Figure 4.7. Finally, the percentage difference in the real components of the eigenvalues and the imaginary components of the eigenvalues were computed in order to determine how the magnitude of the oscillation and damping behaviour varies between the various sets of assumptions. These percentage differences can be seen in Table 4.2. If the difference was found to be reasonably small (about less than 25%), then the corresponding set of assumptions is deemed to be acceptable. From the discussion on the results presented below, it was clear that the eigenvalues outputted by the state space system showed desired results compared to the analytically computed eigenvalues. Therefore, this module test was passed.

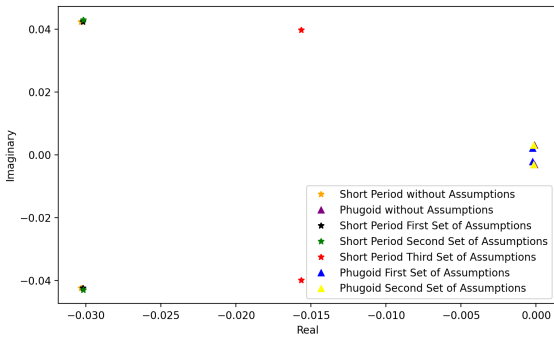


Figure 4.4: Eigenvalues for Symmetric Case (both Complete and Simplified EOM)

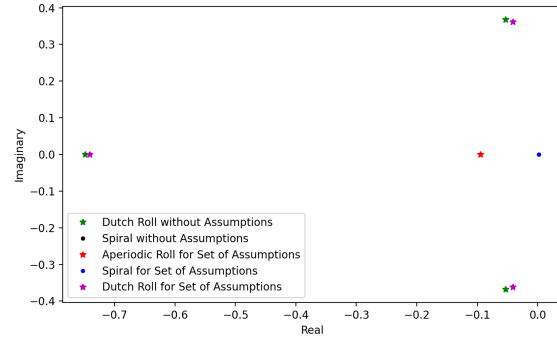


Figure 4.5: Eigenvalues for Asymmetric Case (both Complete and Simplified EOM)

Table 4.2: Percentage Differences of Plotted Eigenvalues

Motion	Assumption	$\Delta\%$ of Real Part	$\Delta\%$ of Imaginary Part
Short Period	1	0.4	0.1
	2	0.4	1.4
	3	48.4	6.1
Phugoid	1	111.4	31.4
	2	36.6	0.8
Dutch Roll	-	1.0	0.0
	-	22.6	1.5
Spiral	-	2.5	0.0
Aperiodic Roll	-	683.3	0.0

Looking at the results, it should be noted that the eigenvalues of the phugoid motion and the short period motion for the third set of assumptions are above the threshold. The reason for the discrepancy of the phugoid motion is due to the eigenvalues being small, resulting in catastrophic cancellation. This is clear from Figure 4.4, as in this figure these eigenvalues are very close. Furthermore, the third set of assumptions for the short period motion has a significant impact on the output of the model, resulting in errors that are outside the predetermined bounds, which can also be seen in Figure 4.4. However, this was expected, since this was also the case for the Cessna Citation I. Finally, it is important to notice that, due to the large set of assumptions used for the aperiodic roll motion, also here a large discrepancy was found in the eigenvalue of this motion for the simplified system. This was, however, also expected from the results on the Cessna Citation I.

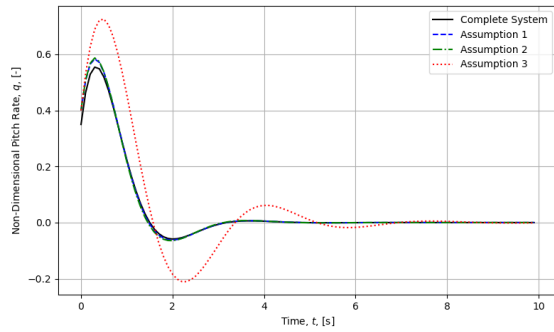


Figure 4.6: Eigenmotion of Complete and Simplified System for Short Period Motion

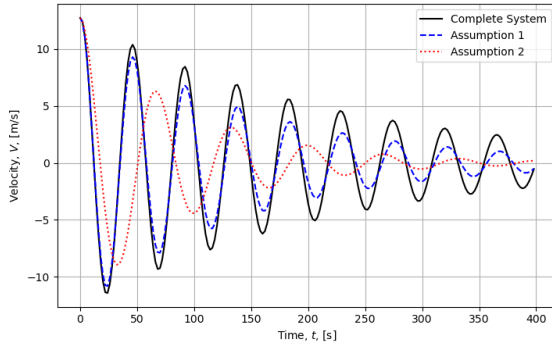


Figure 4.7: Eigenmotion of Complete and Simplified System for Phugoid Motion

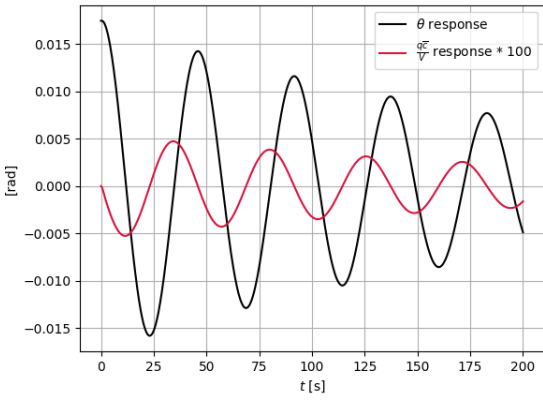
4.6 Global Tests

A final verification of the model is performed by considering systems of the algorithm are performed. The purpose of such tests is to verify that the behaviour of the model is physical and that the expected behaviour is obtained. This kind of model cannot be easily compared to a full analytical solution, as even simple problems are complex to solve entirely by hand.

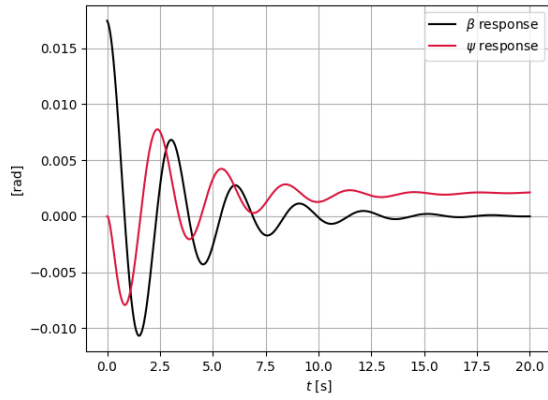
4.6.1 SYS-GLOBAL-001: Initial Value Problem *Alex,Julie*

The numerical model that was developed earlier chapter 2 will be tested by the use of the initial value problem. For the symmetric motion model, input in θ of 1 degree is given. For the asymmetric motion, inputs in ψ and β of the same magnitude will be given. Then the state response of the system will be analysed.

As can be seen from Figure 4.8a, the response of the system is in agreement with the eigenvalues of the numerical model Table 4.1. The response is an underdamped decaying oscillation, which can be expected since the eigenvalues have negative real part and non-imaginary part. The $\frac{q_C}{V}$ response, which has been scaled for visibility, is also in agreement with the pitch angle response, considering it is a scaled-down temporal derivative of it.



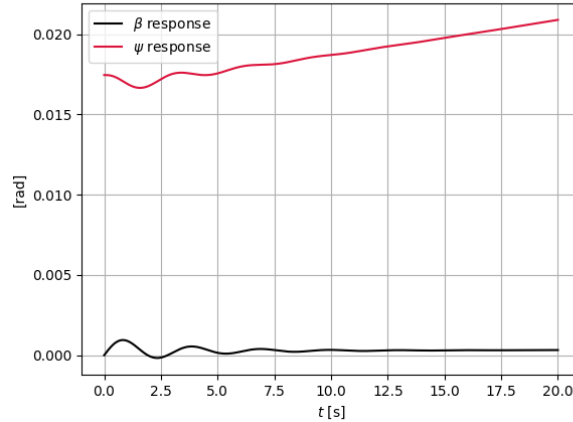
(a) Initial Response to 1 degree deflection in pitch angle



(b) Initial Response to 1 degree deflection in sideslip angle

Figure 4.8: Initial value response for asymmetric model

Regarding the asymmetric response, from the Figure 4.8b it is already clear that the roll response is strongly coupled to the sideslip angle response. Interestingly, even though the sideslip angle response dampens out quite quickly and decays, the roll angle continues to grow exponentially after the initial oscillation has decayed. Once the roll angle reaches large numerical values, it will also cause the roll angle to grow due to the coupling between those two parameters. Similar behaviour is displayed in Figure 4.8c. The non-dimensional roll and yaw rates also show consistent behaviour as temporal derivatives of roll and yaw (sideslip) angles (not shown due to visibility).

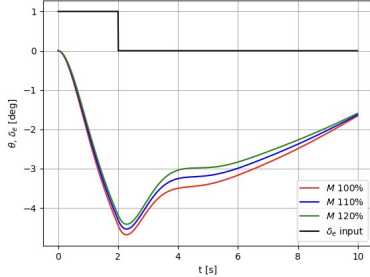
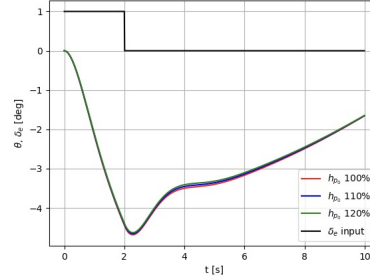
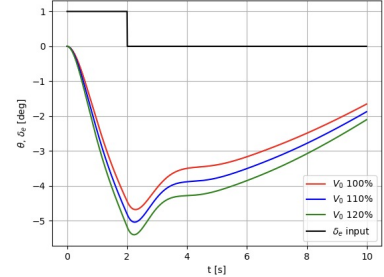


(c) Initial Response to 1 degree deflection in yaw angle

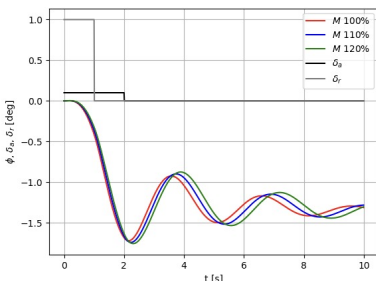
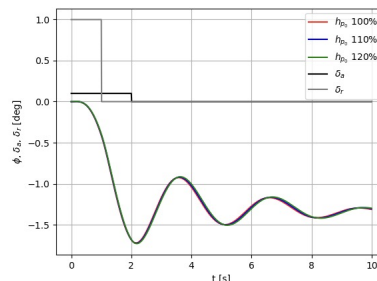
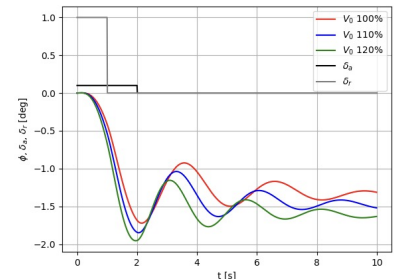
Figure 4.8: Initial value response for asymmetric model

4.6.2 SYS-GLOBAL-002: Sensitivity to Input Values *Lorenz*

An analysis of the model sensitivity is extremely important if the software is to be used in the design phase of a small business aircraft in the future. For this purpose, the behaviour of the model is considered by varying the mass, the altitude and by 10 and 20%, Figures 4.9-4.11 give the sensitivity of the model by considering the change in pitch rate in the short period.

Figure 4.9: Reaction to elevator input
for different massesFigure 4.10: Reaction to elevator input
for different altitudeFigure 4.11: Reaction to elevator input
for different initial velocities

The figures given help to understand the behaviour of the model under such sensitivity, however, for changes of 1% in mass, altitude and velocity, the maximum percentage difference was found to be 0.985%, 0.17% and 2% respectively. This particularly means that the special care should be taken when considering the velocity as it is the most sensitive parameter feeding the simulation in terms of initial state of the aircraft. Similarly, sensitivity on the asymmetric model was performed by considering both an aileron and rudder input.

Figure 4.12: Reaction to aileron and
rudder input for different massesFigure 4.13: Reaction to aileron and
rudder input for different altitudeFigure 4.14: Reaction to aileron and
rudder input for different initial
velocities

For the asymmetric system, changes of 1% in mass, altitude and velocity, the maximum percentage difference was found to be 2.2%, 0.4% and 3.8% respectively. Clearly, this system is more sensitive than the symmetric model, but the variables range in the same way in terms of sensitivity. Again, care must be taken in the initial value of velocity, particularly.

Concluding, the use of the model for preliminary design stage of an aircraft should be done carefully with respect to the velocity, particularly as drawing conclusions from a relatively sensitive parameter can lead to errors in a later design stage. Furthermore, the model being linear, a change in the input values will lead to a linear change in the output values (1% change in the inputs leads to 1% change in the input).

4.7 Test Accuracy Julie, Oliver, Joao, Lorenz, Niek

First, the tests used for the verification of the unit converters and the reduction of the measured speed will be discussed in terms of their accuracy. Firstly, unit test UNIT-CONV-001 is deemed to be very accurate, since the implemented unit test in the code was cross-checked with official conversions available online, which are standard and 100% accurate. Furthermore, regardless of the flight conditions and manoeuvres which take place, the unit conversions will remain consistent. Therefore, the high accuracy should remain consistent for all the data. A similar conclusion can be reached for the unit test UNIT-CONV-002, in which temperature, velocity and other measurements are reduced to standard convention.

Now, looking into the accuracy of the performed tests for the mass and centre of gravity calculation, presented in section 4.2, it can be said that these have an accuracy close to a 100%. This is due to the fact that all the unit tests were compared to hand calculations.

The data used for the lift drag polar and elevator trim curve came from the averaged stationary measurements performed during flight. This information was later processed by converting all units to SI units and reducing all possible parameters to standard condition. Since the unit conversion functions was already verified on UNIT-CONV-001, the accuracy of this part is identical to the latter. Similarly, the reduction parameters were also processed by making use of functions that were previously tested, namely on UNIT-CONV-002. Moreover, several sanity checks were performed during the development phase to guarantee a correct implementation of the code.

Furthermore, a few sanity checks were performed on the recorded inputs data, δ_e , δ_a , δ_r , in order to verify that the data was acquired correctly. This test was conclusive as the sign of the aileron and rudder inputs were found to have been recorded using a different convention and the sign was corrected. This test, however, only intended to verify the consistent sign conventions between the acquired data and the model and never aimed to assess the quality of the measurements. The quality of those measurements is assumed to be good enough for the purpose of the work presented here.

The accuracy of the performed verification steps for the state space model and simplified eigenmotions, discussed in detail in section 4.5, will now be examined. First, the performed unit and module tests to check the right implementation of the state space model will be reviewed. Unit test UNIT-STATE-001 is 100% accurate since the visual checking was done by multiple people, which ensures no mistakes were overlooked. Furthermore, since unit test UNIT-STATE-002 checks the sign of the real part of the outputted eigenvalues, with what is expected from the theory behind the eigenvalues and the stability characteristics of the Cessna Citation II (C550) also this unit test is 100% accurate. Finally, the exact values of the eigenvalues obtained from the state space model are checked by module test MOD-STATE-001. This module test is also very accurate since it uses the implementation of theoretical methods, which are 100% correct. Furthermore, also the implemented characteristic equations used for the test were visually checked by multiple people to avoid errors in the test itself. However, this does not check if the inputs used for the state space model are correct. Therefore, the confidence of the module test is decreased a bit. Finally, the accuracy of MOD-STATE-002 will be discussed. This test is moderately accurate, since the exact values of outputted eigenvalues by the state space model cannot be checked. However, this module test gives a good insight in the magnitude of the eigenvalues. Moreover, since the eigenvalues of the simplified EoM are calculated analytically, this module test can filter large errors in the numerical implementation of the state space model.

Now also the global tests should be commented on in terms of their accuracy. First, the initial value tests performed will be discussed. These tests were done to see if the numerical model shows the behaviour as was expected from theory. However, because this does not check the exact values of the responses, this is only a sanity check made to check the physical behaviour of the model. Considering the sensitivity analysis, such test was performed to assess the reliability of the model on certain parameters as well as its robustness and did not aim to assess its accuracy.

Finally, the coverage of the verification will be discussed in more detail. Apart from the thrust calculation, which was obtained by running a macro, the other parts of the code were checked and verified to ensure the correct functioning of the numerical model. However, to account for overlooking some parts of the numerical model, a decrease of the coverage was taking into account. From this, the coverage of the numerical model verification was estimated to be around 75%.

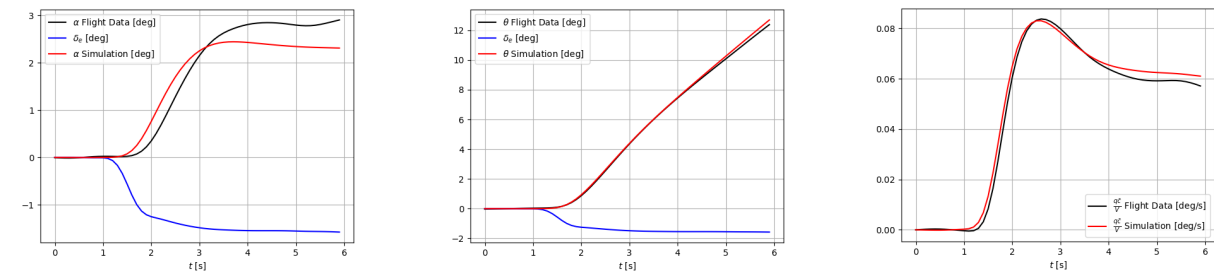
Validation 5

With the data processed, the output of the numerical model can be compared to the experimental data for validation purposes. To validate the numerical model, two steps were taken. First, in Section 5.1, the graphs presenting the experimental data and the data of the numerical model were compared. This will serve as a visual confirmation and can be used to find large discrepancies between the model and experimental data. Subsequently, in Section 5.2 the time to half-amplitude $T_{\frac{1}{2}}$, the undamped natural frequency ω_0 , and the damping ratio ζ of the experimental data and the numerical data will be compared for the Phugoid and Dutch Roll to get a more detailed insight into the approximation of the numerical model. These values can then be compared against each other quantitatively to give a numerical measure for the error between the model and experimental data. Moreover, the improvement of the numerical model by tuning the stability coefficients is presented and discussed in Section 5.3. Finally, some recommendations are presented in Section 5.4.

5.1 Comparison of Graphs for Experimental and Simulation Data *Julie, Alex*

In this section, the experimental data and the simulation output will be compared. This will be done for all the different eigenmotions, executed during the flight. Important to notice is that the inputs to the numerical model are the same as the inputs given by the pilot during the flight. This was done to avoid discrepancies due to different inputs.

First, the results for the short period eigenmotion, presented in Figure 5.1 will be discussed in more detail. From visual inspection of Figures 5.1b and 5.1c it is concluded that both the pitch angle θ , and the non-dimensional pitch rate, $\frac{q_c}{V}$, for the short period can be estimated accurately. However, when looking at the simulation results for the angle of attack, α , shown in Figure 5.1a, the simulation failed to accurately determine these parameters. The difference in the angle of attack can be explained by the fact that the angle of attack measured by the instrumentation on the aircraft does not measure the angle of attack at the centre of gravity, due to the position along the fuselage, whereas the angle provided by the simulation is modelled such that the output is based with respect to the centre of gravity. Furthermore, the aerodynamic flow interacts with the fuselage and other rigid parts of the aircraft before it is measured by the AoA vane. This leads to measurements that relatively deviate from the simulated outputs. At the same time, this deviation is only limited to approx. 0.5° . Important to notice is that alpha will be tuned in section 5.3 in order to obtain a better match with the flight data.



(a) Comparison of α for the Short Period (b) Comparison of θ for the Short Period (c) Comparison of $\frac{q_c}{V}$ for the Short Period

Figure 5.1: Comparison between the Flight Data and Simulation of the Phugoid Eigenmotion Parameters

Subsequently, looking at the results for the phugoid, presented in Figure 5.2, it is clear that the simulation for this eigenmotion again shows discrepancies in the approximation of the angle of attack, as can be seen from Figure 5.2a. The reasoning for this difference is the same as was explained for the discrepancy in angle of attack observed in the simulation for the short period. Furthermore, from visual inspection of Figure 5.2b it is clear that the numerical model is able to capture the change in the pitch angle, θ , quite close except from a small difference in amplitude and a growing offset over time. This can be due to the fact that the initial response of the numerical model shows a higher amplitude compared to the flattened experimental data response to the input. Due to the fact that the input given by the pilot is imperfect, and the aircraft is a way more complex system than the linearized model, the response to this input is different, which leads to discrepancies between the experimental and flight data.

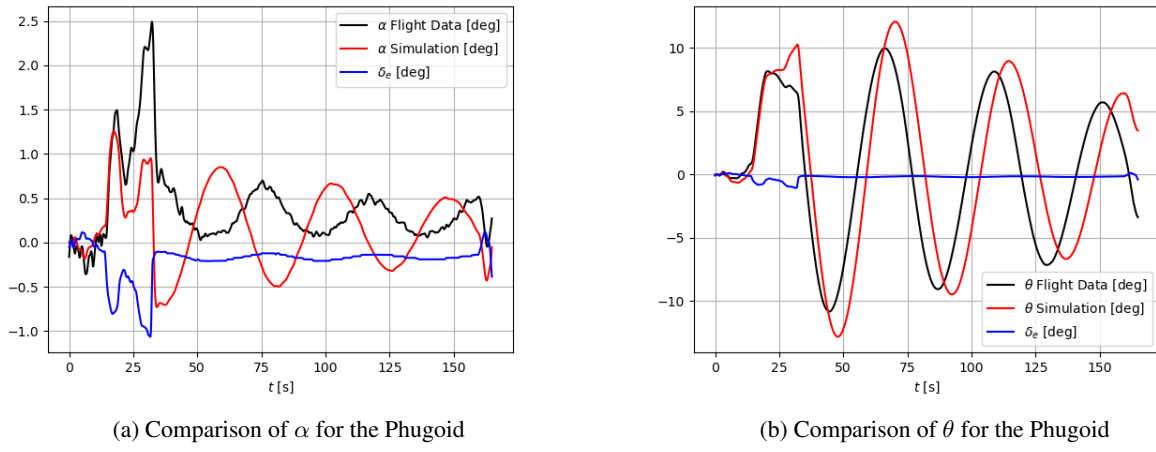


Figure 5.2: Comparison between the Flight Data and Simulation of the Phugoid Eigenmotion Parameters

Now, in the Dutch Roll eigenmotion, the numerical model matches the flight data quite closely, as can be seen in Figure 5.3. The initial response of the numerical model to the doublet rudder deflection has a smaller amplitude compared to the initial response of the experimental data. This can be explained by the fact that because the input given by the pilot is imperfect, and the aircraft is a way more complex system than the linearized model, the response to this input is different, leading to these discrepancies. More specifically, this leads to a faster decay compared to the flight data. Furthermore, this also leads to some phase shift between the two measurements, even though the natural frequency of the eigenmotion seems to be relatively consistent between them.

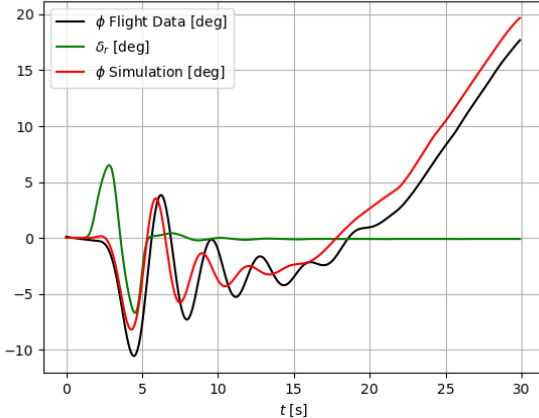


Figure 5.3: Comparison of ϕ between the Flight Data and Simulation for the Dutch Roll

For the aperiodic roll eigenmotion, there is a close match for both the roll angle and non-dimensional roll rate. Both the flight and numerical model data responds correctly to the aileron input. The roll rate changes its sign at the same time the aileron is deflected in the other direction, as can be seen from Figure 5.4b, and consequently the roll angle stops growing and starts decreasing in Figure 5.4a. However, the small difference in the roll angle, ϕ , can be related to the fact that small angle approximations were used in the numerical model, while the roll angles experienced by the aircraft are not in agreement with this assumption, as can be seen in Figure 5.4a. Furthermore, in the graph showing the roll rate, $\frac{pb}{2V}$, the simulation data seems to be parallel to the flight data, this can be due to the fact that the data is not trimmed perfectly.

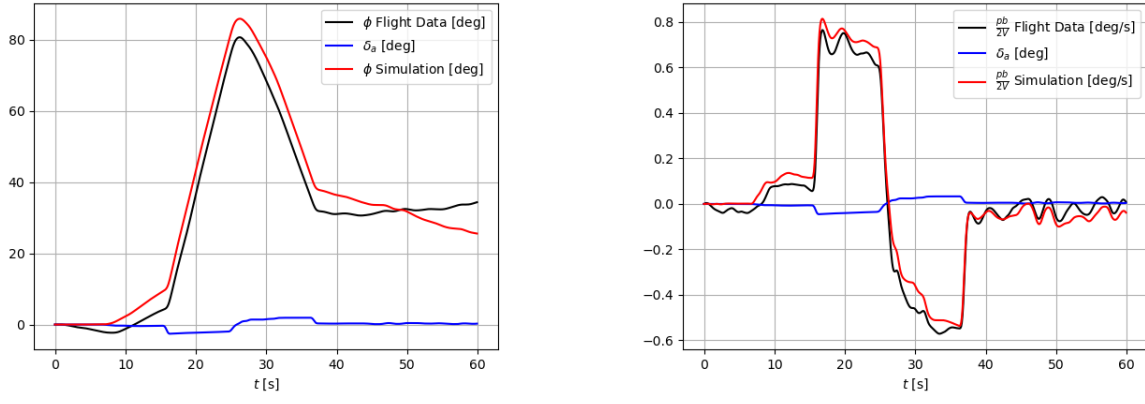


Figure 5.4: Comparison between the Flight Data and Simulation of the Aperiodic Roll Eigenmotion Parameters

Finally, comparing the flight data with the numerical model output for the spiral eigenmotion, in Figure 5.5, it can be seen that most stability characteristics show a close match. However, the roll rate is shifted in the y-direction. This could be explained by the initial response of the simulation, which causes an increase in roll rate while the flight data roll rate decreases. This initial discrepancy causes a shift for the whole measurement duration. It should be noted that for the spiral manoeuvre the roll rate is not of the most importance, as it has limited amplitudes in the order of < 0.1 [deg/s]. The initial response of the model needs further investigation, however it is difficult to compare it with the flight measurements as giving a perfect input is not possible in reality.

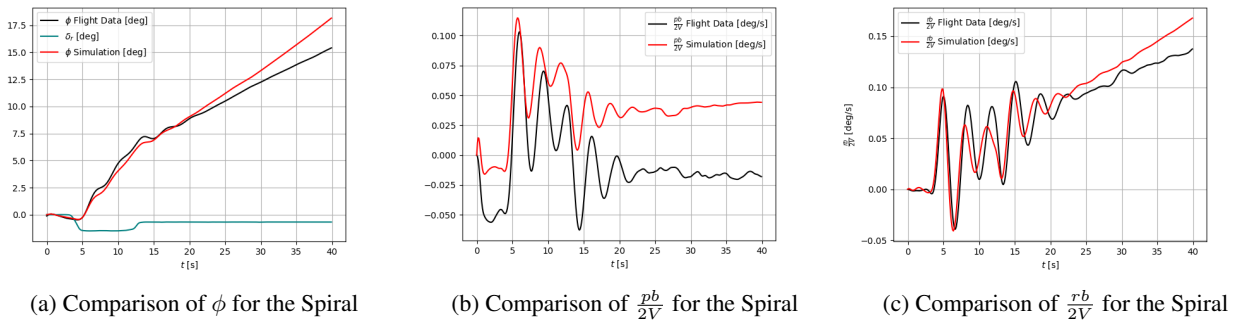


Figure 5.5: Comparison between the Flight Data and Simulation of the Spiral Eigenmotion Parameters

5.2 Comparison of Eigenmotion Parameters of Experimental Data and Numerical Model Output *Alex,Julie*

The relevant parameters for the flight data can be seen in Table 3.8, and the numerical model characteristics are obtained from the eigenvalues of equations of motion for the symmetric and asymmetric cases, by performing numerical operations with the real and imaginary parts of the complex eigenvalues. Since both part of the numerical model will be tested, two eigenmotions are deemed sufficient for this validation step.

Table 5.1: Eigenmotion characteristics as derived from the flight data and from complex eigenvalues of symmetric and asymmetric motions. Obtained using the method outlined in [1, ch.5-6]

Eigenmotion	$T_{1/2}$ [s]	ω_0 [rad/s]	ζ []
Phugoid FD	154	0.149	0.03018
Phugoid NM	157.154	0.1376	0.032
Difference [%]	2.05	-7.65	-6.03
Dutch Roll FD	3.79	1.8	0.10114
Dutch Roll NM	2.2881	2.065	0.1432
Difference	-39.6	14.72	29.4

As can be seen from Table 5.1, for the Phugoid eigenmotion there is a strong agreement between the flight data and the numerical model, especially while taking into consideration the presence of numerous assumptions explained in section 2.3. This shows that the numerical model is capable of accurately predicting the characteristics of the Cessna Citation II (C550) during a phugoid. Furthermore, comparing the undamped natural frequency, ω_0 , for the Dutch Roll, the 14.72% difference is assumed to be quite accurate taking into the account all the assumptions and the fact that the numerical model is linearized. In the asymmetric equations of motion, there is a conjugate pair of complex eigenvalues and two distinct real eigenvalues. Only the complex eigenvalues were used to calculate the Dutch Roll numerical model characteristics, which could lead to large errors in time to half amplitude and damping ratios, as can be seen in Table 5.1. However, the difference of up to 40 % is considered acceptable given the fact that impact of real eigenvalues was discarded and in real flight all the effects (corresponding to different eigenvalues) combine.

5.3 Improvement of Numerical Model: Model Matching *Oliver, Joao*

In this section, an attempt to tune the simulation is presented in order to better replicate the data which was measured in the flight test. This was done via a trial and error method which, following numerous iterations, allowed for the determination of the optimal values of the various stability and control derivatives which are used in the symmetric and asymmetric equations of motion. These optimized values are shown below on Table 5.2 (note that all variables not included here remain unchanged from the original Cit_par22.py code provided on Brightspace).

Table 5.2: Symmetric and asymmetric stability and control derivatives numerical values

	Before	After
C_{X_α}	0.47966	0.46530
C_{Z_u}	-0.37616	-2.50000
C_{m_u}	0.06990	0.00000
C_{Y_b}	-0.75000	-0.98960
C_{Y_β}	0.00000	-10.00000
C_{Y_p}	-0.03040	-0.08700
C_{n_p}	-0.06020	-0.08500
C_{n_r}	-0.20610	-0.19300

The modification of the stability and control derivatives for optimization obeyed the following procedure: following the system matrices, individual stability and control derivatives were replaced with an extreme value in order to reveal how they impact the nature of the model response to the various manoeuvres of the flight. After understanding the nature of the impact, the variables were returned to their original value and then subsequently changed to a value which allowed for the simulation to better replicate the actual results. To get an idea of the range of possible values which are typical for stability derivatives in comparable aircraft, data from Cit_par22.py and Table D-1 from Appendix D of [1] (provides the symmetric and asymmetric stability and control derivatives for the Cessna Ce500 for cruise condition) were used as reference. In certain cases, it was found that the adjustment of certain parameters allowed for the model improvement in certain specific responses while compromising the performance in areas. If this couldn't be compensated with the adjustment of other parameters, then a balance had to be established. This is where the iterative nature of the adjustments becomes important.

The parameters shown in Table 5.2 denote the variables which required the most significant amount of adjustments. For the symmetric flying case, the most noticeable changes in stability values were found to be in the parameters C_{Z_u} and C_{m_u} . This was done in order to significantly improve the irregular behaviour of the angle of attack response for the phugoid motion. However, this was found to negatively affect the remaining characteristic responses. Therefore, for the tuning of the symmetric response, it is important for the user to keep in mind which elements of the response they are looking to simulate, as the selection of optimized parameters should be adjusted for those sets of data.

In contrast to the symmetric case, a certain combination of stability and control derivatives lead to a global improvement across all stability response. The most noticeable change in these parameters is that of C_{Y_β} . In lectures, this variable was assumed to be zero. However, in the asymmetric flying case, it was found that this derivative in particular played a crucial role in ensuring model matching the simulation to the data. This is because the adjustment of this variable was found to have a profound impact on the phase shift of the asymmetric response. Therefore, a significantly different value of this stability parameter allowed for the simulation to perfectly match the phase of the roll rate, bank angle and the yaw rate. This can be clearly seen in the difference between the original and tuned response shown in Figure 5.6. While it is understood that such an extreme value for this parameter is most likely not representative of physical aircraft properties, this was kept simply for the aim of comparison. Asides from this change, C_{Y_b} , C_{Y_p} , and C_{n_p} were adjusted to further

improve the performance of the yaw rate and roll rate specifically. These effects, however, we found to be more minor. With this combination, the simulated response was found to match the experimental data as close as possible.

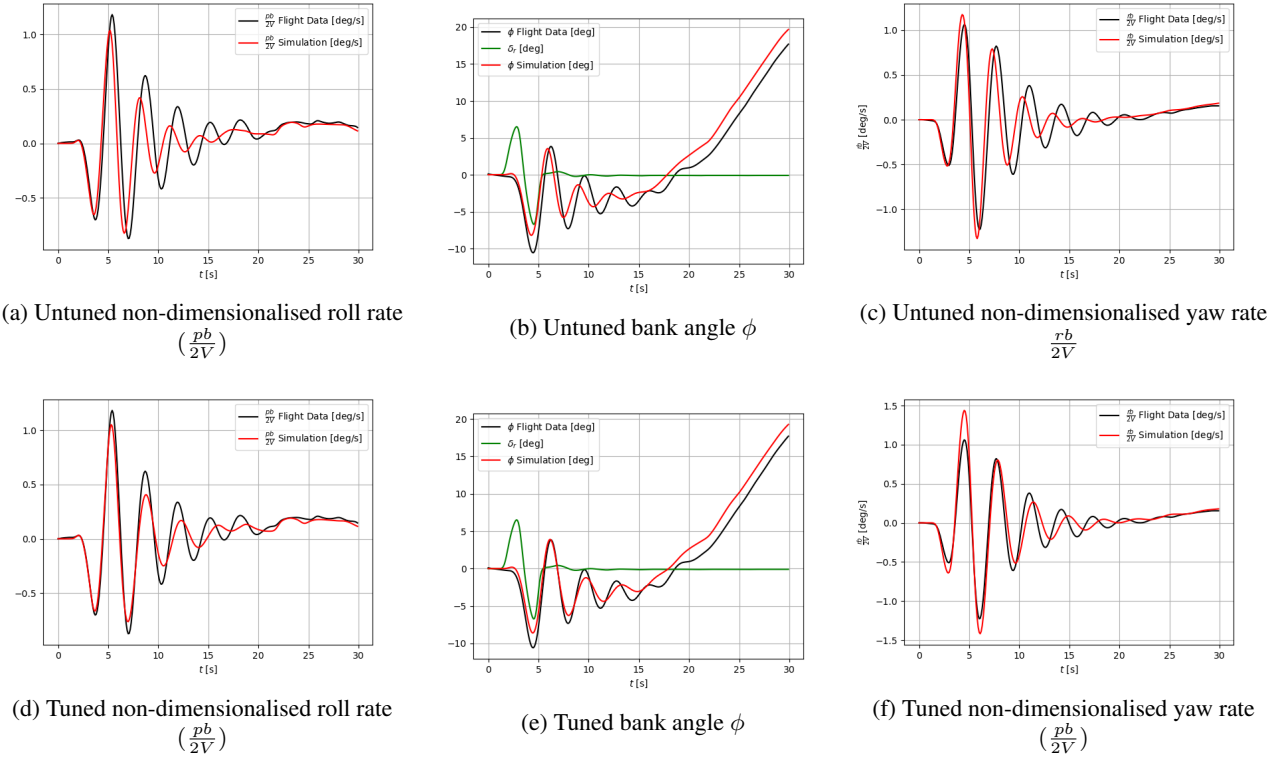


Figure 5.6: Results for unsymmetric tuning for Dutch Roll

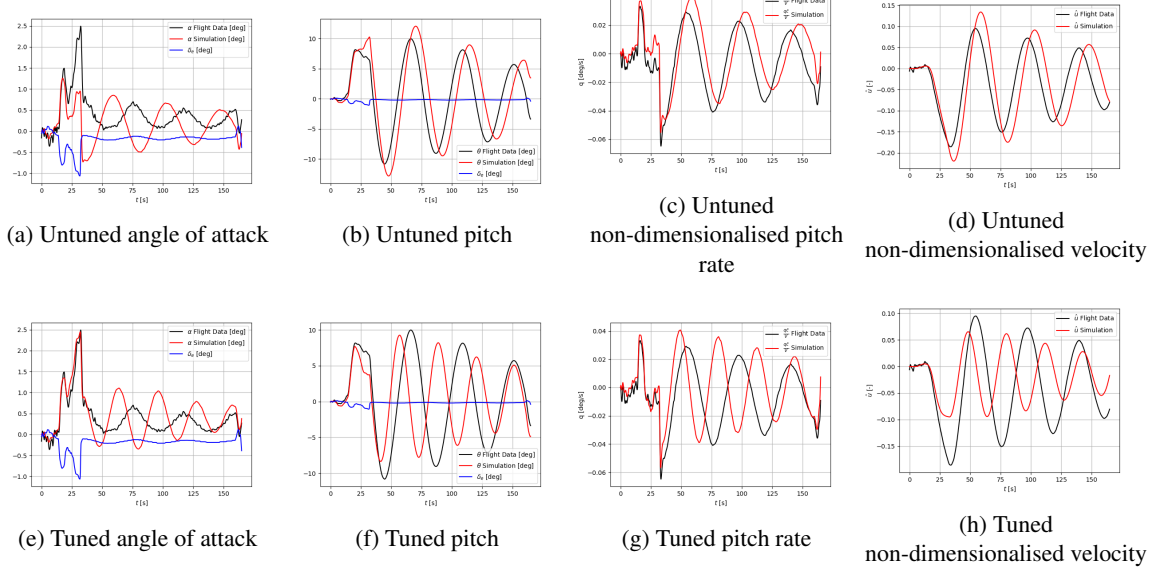


Figure 5.7: Results for symmetric tuning for Phugoid

5.4 Reflection Numerical Model *Alex*

Overall, the numerical model shows satisfactory performance, as the match with flight data is extremely good for the most part. The model is built with a series of assumptions in mind, and reducing the impact of those assumptions is likely to lead to an even better match. For the dynamic response of the aircraft, assumptions **GA-04**, **GA-06** and **GA-11** are likely to have the most impact. Assumption **GA-11** would be the hardest to change, since the numerical model currently employed is inherently linear. Removing this assumption would mean that a completely new model is needed. Assumptions **GA-04**

and **GA-06** are both affected by the fact that thrust in both engines during the flight test was not equal, which would cause the weight of the fuel in the two wings to be different and also shift the thrust vector laterally. The numerical model can be expanded at relatively low cost to take fuel flows as inputs and calculate resultant changes in thrust direction and moments of inertia. This would also allow for better comparison with test flight data, as those effects will be accounted by the model.

The numerical model also takes stability characteristics derived from the stationary measurements as its parameters. Thus, an error in those parameters would also lead to an error in dynamic measurements. Assumptions **GSA-01** and **GSA-04** are likely to cause a significant error in those measurements. First of all, it was not confirmed whether the horizontal stabilizer has a symmetric airfoil. If it doesn't, additional computations need to be carried out to account for the M_{ac} , moment around the aerodynamic centre. Secondly, it is assumed that the thrust of the engines is aligned with the body axis of the aircraft, but this is likely not the case. Engines at the back are likely to contribute a nose-down moment, which was not accounted for in the derivation of static stability characteristics. Removing those two assumptions would likely have a strong improvement on the accuracy of the stationary measurements.

It is recommended to improve the performance of the numerical model through the stationary measurements first, as this is easier and requires fewer changes to the program. It will also implicitly improve the performance of the numerical model for the dynamic measurements as well. To summarize, the first improvement should be accounting for the installation angle of the engines and the moment caused by that (**GSA-04**), afterwards the moment around the aerodynamic centre of the elevator should be checked (**GSA-01**). Once those two static effects are accounted for, accounting for uneven fuel flow and hence thrust would further improve the model and allow for better comparison with flight data (**GA-04**, **GA-06**). In case even better performance is needed, non-linear effects and aerodynamic interactions and coupling of aerodynamic parameters needs to be incorporated in the numerical model **GA-11**.

Conclusion 6

The purpose of this report is to document the development, verification and validation of flight simulation software for the small business jet aircraft, taking Cessna 550 Citation II as a reference. The theoretical derivation of the numerical model used for the simulation is given in Chapter 2, the processing of the flight test data is explained in Chapter 3, verification of the flight dynamics software is documented in Chapter 4, and finally the validation is explained in Chapter 5.

The flight dynamics software developed has completed several unit, module and global verification tests and validation through qualitative (eigenmotion plots) and quantitative (comparison of natural frequency, damping ratio, time to half amplitude) comparison with post-processed flight data. Verification tests were passed, and a good match has been achieved with experimental measurements, which leads to the conclusion that this software can be used in the preliminary design of the business jet with similar configuration to the reference aircraft. It can serve as a cheap and effective design tool to give engineers an insight to the stability and dynamic response of the aircraft. Because the program uses a linear model, the computational effort is cheap and many various aircraft configurations can be tested at the conceptual design stage, in order to achieve an optimized design.

At the same time, the software does not achieve very high accuracy when compared with the flight data, and there is still room for improvement. Increase in accuracy can either be achieved through expansion of the software to reduce the number of the underlying assumptions, or through tuning of stability parameters to achieve a better match with the flight data. Both approaches are explained in more detail in section 5.3. A more radical solution is also to use a non-linear model, however this would lead to a much higher cost of program development and also computational effort when running it.

This report serves as an official documentation to the simulation software. All the code has been published on the TU Delft GitLab page, and an overview of the code structure is given in section 2.6.

References

- [1] J. Mulder *et al.*, *Flight dynamics*, TU Delft, Mar. 2013.
- [2] E. Cruiser. “Airplane’s body, stability and wind axis.” (Sep. 2011), [Online]. Available: <https://dodlithr.blogspot.com/2011/09/airplanes-stability-axis.html>.
- [3] M. Crombaghs, E. de Min, and G. van Hees, *The first absolute gravity measurements in The Netherlands*. P.O. Box 5030, 2600 GA Delft, The Netherlands: NCG, Nederlandse Commissie voor Geodesie, Netherlands Geodetic Commission, Delft, The Netherlands, 2022.
- [4] A. in ’t Veld and T. Mulder, *Flight dynamics assignment ae3212-ii*, TU Delft, Mar. 2022.
- [5] P. Roling and A. in ’t Veld, *Thrust calculation excel sheet*, 2022.
- [6] J. Anderson, *Introduction to Flight*, 8th international ed. New York, United States: McGraw Hill Education, 2016.
- [7] J. Ruijgrok, *Elements of Airplane Performance*, 2nd ed. Delft, the Netherlands: Delft Academic Press, 2013.
- [8] B. H. Thacker, S. W. Doebling, F. M. Hemez, M. C. Anderson, J. E. Pepin, and E. A. Rodriguez. “Concepts of model verification and validation.” (2004), [Online]. Available: <https://www.osti.gov/servlets/purl/835920-YI8Ow3/native/#:~:text=Model%5C%20verification%5C%20and%5C%20validation%5C%20are,building%5C%20credibility%5C%20in%5C%20numerical%5C%20models.&text=Validation%5C%20is%5C%20the%5C%20process%5C%20of,intended%5C%20uses%5C%20of%5C%20the%5C%20model>. (visited on 03/18/2022).